EES Catalysis

REVIEW ARTICLE

View Article Online
View Journal | View Issue

Cite this: *EES Catal.*, 2024, 2, 138

Photocatalytic inactivation technologies for bioaerosols: advances and perspective

Linghui Peng,[ab] Haiyu Wang,[ab] Yuelong Wang,[ab] Guiying Li [ab] and Taicheng An *[ab]

Received 25th July 2023,
Accepted 7th September 2023

DOI: 10.1039/d3ey00179b

rsc.li/eescatalysis

Bioaerosol control systems are urgently needed to inactivate airborne pathogenic microorganisms to prevent secondary contamination. Recently, with an increasing number of studies on the characteristics of bioaerosols, researchers have gained a better understanding of bioaerosols, which has promoted the development of bioaerosol control technology. Bioaerosol photocatalytic inactivation technology shows its superiority through excellent oxidation capacity, environmental friendliness, the absence of secondary contaminations, and good compatibility. However, there are very few available studies that comprehensively summarize and present the state of bioaerosol photocatalytic inactivation technology. This article mainly reviews the recent advances in advanced materials, combined technologies, carriers and reactors, applications and performance evaluations of photocatalytic inactivation technology. The efficiency, advantages and disadvantages of these factors are comprehensively discussed. This review also highlights the practical applications, addresses the challenges, and provides a perspective on bioaerosol photocatalytic inactivation for future research.

Broader context

Bioaerosol control technologies have attracted more and more research interests due to increasing demands for the reduction of bioaerosol hazards, especially in the situation of the quick spread of the COVID-19 pandemic. As one of the most promising technologies, bioaerosol photocatalytic inactivation technology emerged in 1995, 10 years after its application in the field of water sterilization due to lack of understanding of the characteristics of bioaerosols. Recently, with increasing research on the characteristics of bioaerosols, researchers have gained a better understanding of bioaerosols, which has promoted the development of bioaerosol control technology. Bioaerosol photocatalytic inactivation technology shows its superiority through excellent oxidation capacity, environmental friendliness, the absence of secondary pollution, and good compatibility. However, there are no available studies that comprehensively summarize and present the state of photocatalytic inactivation technology for bioaerosol control, which is quite different from water disinfection. This article mainly reviews the recent advances in the design of efficient photocatalysts, classifications of photocatalyst carriers and reactors, applications of photocatalysts and performance evaluations for bioaerosol inactivation and is expected to contribute to a better understanding of the development and the achievement of highly efficient control of bioaerosols.

1. Introduction

Bioaerosols have been studied for about 200 years since 1833 when mold spores were first detected in the air by Charles Darwin.[1] In recent decades, there has been a research boom in the bioaerosol field, thus triggering many research studies aimed at understanding "what is bioaerosol (classification)", "why we should control it (harm)" and "how to control it (control technology)" (shown in Fig. 1). Bioaerosols contain complex pathogenic microorganisms no matter in indoors or outdoors,[2,3] including bacteria, fungi, viruses, pollen, and their derivatives such as allergens, endotoxin, mycotoxins, *etc.*[4,5] The largest mode diameter observed for fungal spores in bioaerosols ranges from 1 to 30 μm, followed by that for bacteria (2–8 μm). The smallest diameter is observed for viruses, measuring about 0.3 μm, while the size distribution of bioaerosols from animal and plant fragments is more varied, ranging from 0.001 to 100 μm.[2,6] The bioaerosols are small enough to linger in air, accumulate in enclosed spaces, deposit on surfaces, and be inhaled in both short and long ranges.[7–9] Humans exposed to bioaerosols are at risk of infections.[10–12] Two major transmission routes for respiratory-borne diseases, namely, short-distance droplet transmission and

[a] *Guangdong Key Laboratory of Environmental Catalysis and Health Risk Control, Guangdong-Hong Kong-Macao Joint Laboratory for Contaminants Exposure and Health, Institute of Environmental Health and Pollution Control, Guangdong University of Technology, Guangzhou 510006, China. E-mail: antc99@gdut.edu.cn*
[b] *Guangdong Engineering Technology Research Centre for Photocatalytic Technology Integration and Equipment, Guangzhou Key Laboratory of Environmental Catalysis and Pollution Control, School of Environmental Science and Engineering, Guangdong University of Technology, Guangzhou 510006, China*

contact with contaminated surfaces (or fomites) have been discovered.[13] Various indoor bioaerosols, especially the infectious microbes, are closely linked with various diseases, such as pneumonia, infectious diseases, cancer, asthma, and allergic diseases.[14] Therefore, bioaerosol control is urgently needed for human health.

Due to the prevalence of respiratory infectious diseases caused by bioaerosols,[15–18] strategies and technologies for bioaerosol control have been intensively investigated.[19–22] Existing bioaerosol control ways include physical, chemical, and biological methods.[16] Physical methods like ultraviolet (UV),[23] thermal,[24] and microwave irradiation,[25] plasma,[26,27] ions,[28] filters[29–31] and static electricity[32–34] can inactivate bioaerosols in enclosed spaces by destroying their genetic matter or their physical structures.[35] They suffer from huge energy consumption, space occupation, and localized inactivation.[20] Disinfectant spray,[36] ozone (O_3),[37] and photocatalysts[38,39] are typical chemical methods for bioaerosol inactivation. Chemical methods can indeed inactivate bioaerosols quickly and cheaply, but usually lead to byproducts that are harmful to humans.[16] With the development of biotechnology, biological enzyme elimination can also realize targeted inactivation of microorganisms with high efficiency without causing secondary pollution.[40] However, biological enzymes only inactivate specific microorganisms, and are not suitable for complex bioaerosol inactivation.

As a clean chemical method, photocatalytic technology shows great potential for the inactivation of airborne biological contaminants due to its excellent oxidation capacity, environmental friendliness, absence of secondary pollution, and good compatibility.[41,42] Photocatalytic sterilization in water began in 1985.[43] Matsunaga *et al.* first reported that Pt-loaded titanium dioxide (TiO_2) can be used to inactivate *Saccharomyces cerevisiae* cells in water, which opened the door to photocatalytic inactivation technology. Photocatalytic inactivation of water microorganisms was then intensively investigated,[39,44–46] because the

Linghui Peng

Dr Linghui Peng is a post-doctoral researcher at the School of Environmental Sciences and Engineering, Guangdong University of Technology, under the supervision of Prof. Taicheng An. She received her PhD from Monash University in 2020. Her research focuses on the photocatalytic inactivation of bioaerosols and bioinspired materials for bioaerosol control. The related works have been published in Nat. Commun., Appl. Catal. B: Environ., and so on.

Haiyu Wang

Mr Haiyu Wang received his masters' degree from the School of Chemistry and Chemical Engineering, North Minzu University, Yinchuan, China in 2020. He is currently pursuing his PhD degree at the Institute of Environmental Health and Pollution Control, School of Environmental Sciences and Engineering, Guangdong University of Technology, China, under the supervision of Prof. Taicheng An. His research interest focuses on efficient bioaerosol control technology.

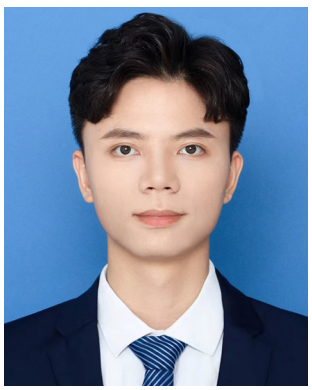

Yuelong Wang

Mr Yuelong Wang received his bachelor's degree from the School of Environmental Science and Engineering, Guangdong University of Technology. He is currently pursuing a PhD in environmental science and engineering at the Institute of Environmental Health and Pollution Control, Guangdong University of Technology. His research interest focuses on the capture and inactivation of bioaerosols.

Guiying Li

Prof. Guiying Li received her PhD degree in environmental science from Griffith University, Australia. She is now a full professor at Guangdong University of Technology. Her academic background encompasses both microbiology and environmental science. Her research interest mainly focuses on the development of photocatalysis and photoelectrocatalysis-based bactericidal methods, and application mechanism of photocatalytic bactericidal decomposition. She has published more than 330 SCI papers in reputed journals, such as Water Res., Appl. Catal. B, ES&T and J. Catal. She is the holder of 70 issued patents and has received the second-place award for the Natural Science Prize from the Ministry of Education (MOE), China.

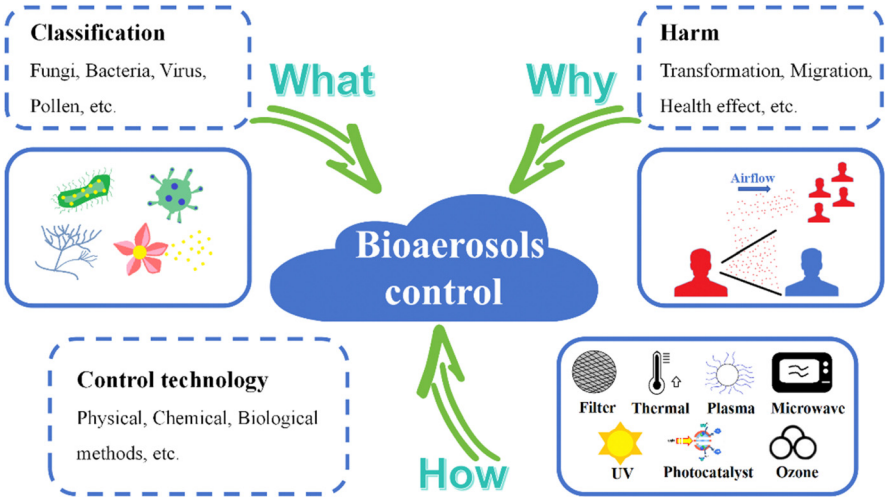

Fig. 1 Illustration of research contents about bioaerosol control.

photocatalysts are low cost, stable, ease of manufacture, and minimally toxic.[47]

However, photocatalytic inactivation of bioaerosol was rarely investigated until 1995,[48] which was 10 years later as shown in Fig. 2. The difficulty in photocatalytic inactivation of bioaerosols lies in their relatively low concentration, compared to disinfection in water. The microbes in bioaerosols cannot fully come in contact with photocatalysts as in water; thus the efficiency of photocatalytic inactivation may be reduced. The pioneering work in the field of gas phase photocatalytic disinfection (bioaerosol inactivation) was done by Goswami *et al.* in 1995.[43] During the first ten years (1995–2005), TiO_2 was mostly used at the beginning of bioaerosol photocatalytic inactivation due to its excellent photocatalysis and easy preparation.[49] The subsequent research shifted toward improving reactor designs, by modifying the size, shape, and structure of the photocatalytic reactors.[50,51] With a deepening understanding of bioaerosol, the photocatalytic inactivation was directly conducted with various types of bioaerosols, including fungi, bacteria, viruses and spores in around 2018.[52,53] As different types of bioaerosols show different size distributions and activity, the inactivation efficiency of various types of bioaerosols is dependent.

In recent times, more and more researchers have devoted their efforts to bioaerosol photocatalytic inactivation in response to the growing demand for bioaerosol control for human health protection.[20,54] Bioaerosol photocatalytic inactivation offers advantages of low cost, environmental friendliness and chemical stability, making it more suitable for bioaerosol control in occupied areas. Contemporaneously, the individual TiO_2 photocatalyst cannot meet the requirement of quick photocatalytic inactivation, leading to the rapid development of combined photocatalysts to enhance the photocatalysis and broaden the range of applications.[55–57] In 2020, the COVID-19 outbreak greatly accelerated the development of bioaerosol photocatalytic inactivation.[58,59] From 2020 to the present, a lot of novel and high-efficient photocatalytic materials have emerged due to the boom in nanotechnology.[60–62] Mxenes,[63] metal–organic frameworks (MOFs),[64] photocatalytic dyes,[65] and metallic oxides[66] are four major types of photocatalysts that have been recently investigated for bioaerosol inactivation. Among them, a special type of bio-inspired photocatalyst has attracted attention; it mimics the structure and morphology of natural plants and animals to improve its bioaerosol photocatalytic inactivation properties.

Studies on classifications, emissions, and health effects of bioaerosols have increased recently.[67–69] However, the available studies have not comprehensively summarized and presented the state of bioaerosol photocatalytic inactivation. This paper reviews the recent advances in the design of efficient photocatalysts, classifications of light sources, photocatalyst carriers

Taicheng An

Prof. Taicheng An is the founding director of the Institute of Environmental Health and Pollution Control, and the Dean of School of Environmental Sciences and Engineering, Guangdong University of Technology, China. He is the winner of the National Natural Science Funds for Distinguished Young Scholars, and Distinguished Professor of Chang Jiang Scholars. He is the recipient of the first award of Guangdong Province and second award for the Natural Science Prize from MOE, China. One of his current research focuses on the application of advanced oxidation processes, especially heterogeneous photocatalysis in biohazard inactivation in water and air. He has published more than 500 SCI papers in reputed journals, such as Nat. Commun., PNAS, JACS. He also served as an Associate Editor for Appl. Catal. B: Environ., and Crit. Rev. Env. Sci. Tec.

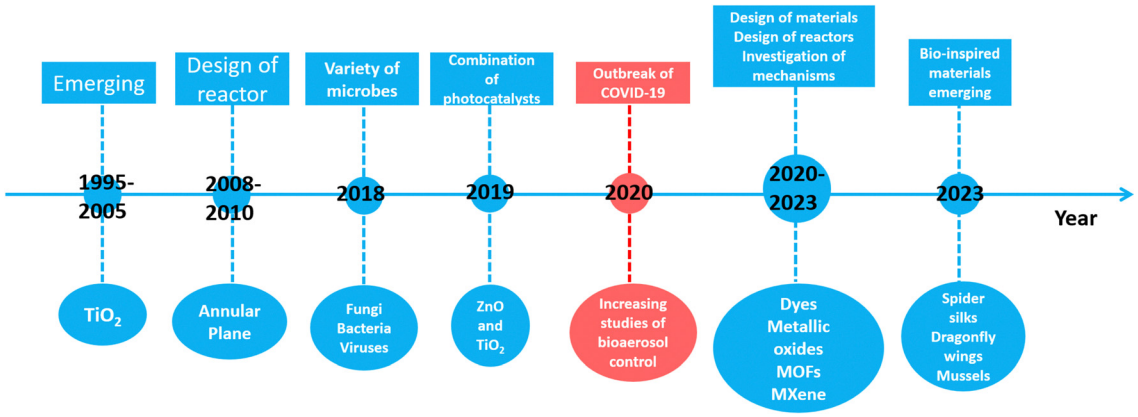

Fig. 2 Development of photocatalysts for bioaerosol control.

and reactors, applications of photocatalysts and the performance evaluations for bioaerosol inactivation. A comprehensive comparison and discussion of different types of photocatalysts have been presented and this review may be expected to contribute to a better understanding of the development and the achievement of high-efficiency bioaerosol control technologies.

2. Photocatalytic technologies for bioaerosol inactivation

Photocatalysis can be defined as the acceleration of a chemical reaction that occurs when a light source interacts with the surface of the photocatalyst.[70] Photocatalysis has been recognized as an impressive green solution technology for applications in microbial disinfection, and it has already been investigated comprehensively in water treatment.[44,71,72] Nowadays, photocatalytic inactivation is applied to bioaerosol inactivation and has been proven to be systematically effective in deactivating a wide range of organisms.[73]

2.1 Photocatalyst materials

Semiconductor metal oxides or semiconductor photocatalysts have exhibited a great photocatalytic performance and have been investigated for a long period.[19] Valdez-Castillo *et al.* developed a perlite-supported ZnO/TiO_2 photocatalytic system with 70% airborne fungal/bacterial inactivation efficiency.[56] As shown in Fig. 3a, TiO_2 nanoparticles with a size of ~20 nm can be used as a functional material to decorate photo-reactors for bioaerosol purification and inactivation.[49] Zacarías *et al.* reported TiO_2-coated glass rings in a fixed-bed reactor for photocatalytic inactivation of *Bacillus subtilis* vegetative cells, achieving a reduction of more than 96% for 12 h.[74] Vohra *et al.* developed an Ag doped TiO_2 platform along with ultraviolet (UV-A) light arrays for photocatalytic inactivation of airborne *Bacillus cereus* bacterial spores in 8 h.[49] After Ag doping, Ag could act as an intermediate agent to enhance the electron–hole separation efficiency of TiO_2, yielding high inactivation efficiency. Lately, Wang *et al.* constructed *in situ* grown NiFeOOH nanosheets on nickel foam for bioaerosol inactivation within 8.07 s under UV irradiation.[75] These novel bimetallic oxyhydroxide NiFeOOH sheets with sharp edges (Fig. 3b) show excellent photocatalytic performance on adding trace O_3 and this combination possesses great potential for bioaerosol inactivation. In addition, the sheet shape of the photocatalyst can also cause physical damage to the bioaerosol apart from photocatalytic oxidation. Semiconductor metal oxides and their composites usually utilize high-energy light for photocatalysis and their electron–hole pairs are easily recombined. As semiconductor metal oxides are known for their chemical and humidity stability with high photocatalytic activity, they show great potential for bioaerosol control and have been extensively investigated in the photocatalytic inactivation of bioaerosols.

With the development of synthesis and design of photocatalytic materials, many novel materials have been applied to bioaerosol photocatalytic inactivation. A new family of two-dimensional early transition metal carbides and/or nitrides (MXenes) has attracted

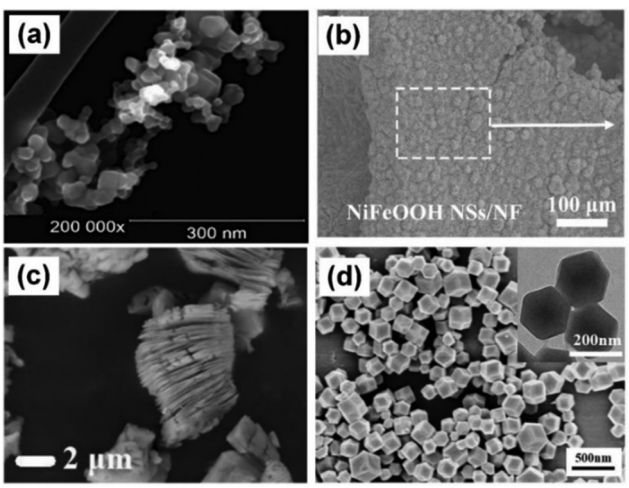

Fig. 3 Morphology of photocatalysts for bioaerosol inactivation. (a) TiO_2 nanoparticles,[56] Reproduced with permission. Copyright 2019, Elsevier. (b) NiFeOOH nanosheets,[75] Reproduced with permission. Copyright 2023, Elsevier. (c) MXene,[63] Reproduced with permission. Copyright 2021, Elsevier. (d) MOF (ZIF-8),[85] Reproduced with permission. Copyright 2022, Elsevier.

intensive interest since their synthesis.[76] The most studied nanosheet among MXenes is $Ti_3C_2T_x$ (T = OH, F or O).[77] Density functional theory (DFT) calculations predict that $Ti_3C_2T_x$ exhibits metallic conductivity, which is favorable for electron–hole separation and charge transfer, indicating better photocatalytic performance.[78] As shown in Fig. 3c, with the special structure of few layered or monolayered nanosheets, MXene may effectively improve the photocatalytic performance.[63,76] Lu *et al.* reported a $TiO_2/Ti_3C_2T_x$ nanosheet-loaded polyurethane foam in a continuous flow-through reactor, which decreased airborne *Escherichia coli* by an order of 3.4-log under ultraviolet irradiation.[63] Recently, the same group designed a dynamic continuous flow photocatalytic reactor containing TiO_2/MXene fillers to study the inactivation characteristics of four different microorganisms when subjected to ultraviolet and photocatalytic treatment.[38] An appropriate residence time (4.3 s) can prove to be efficient in treating airborne microorganisms with higher concentration (10^9 CFU m^{-3}). However, high relative humidity and hard-to-peel layers will inhibit the performance of MXenes.

Metal–organic frameworks (MOFs) are hybrid organic–inorganic porous crystalline nanomaterials that have attracted great attention in environmental remediation due to their crystalline nanoporous (<2 nm) or mesoporous (2–50 nm) structure, extremely high surface area, and significant chemical diversity.[79,80] They have been vigorously investigated in the field of gas storage, separation, and catalysis.[80,81] The large surface area, high porosity, well-dispersed active centers, and tunable functionalities of MOFs make them good candidates not only for volatile organic pollutants purification[82] but also as promising heterogeneous photocatalysts for bioaerosol oxidation.[79,83,84] As shown in Fig. 3d, Ni *et al.* prepared MOF(ZIF-8) particles and presented an air filter composed of keratin-based nanofibers as an upper layer and ZIF-8-modified polyethylene terephthalate/polyethylene fiber mats as the substrate for bacterial inactivation.[85] Li *et al.* prepared a zinc-imidazolate MOF (ZIF-8) with photocatalytic bactericidal properties. Specifically, ZIF-8 exhibits >99.99% photocatalytic killing efficiency against airborne bacteria in 30 min.[64] Zhu *et al.* reported the UiO-66-NH_2/poly[2-(dimethyl decyl ammonium) ethyl methacrylate] composite (UiO-PQDMAEMA) filter, which demonstrates an excellent capability of efficiently killing both Gram-positive (*Staphylococcus epidermidis*) and Gram-negative (*E. coli*) airborne bacteria.[86] Zhang *et al.* prepared a MOF (CAU1-OH) that exhibits a desired working range (40–60% RH), a high working capacity (0.41 g g^{-1}), an excellent cycle performance (500 cycles), and a high photocatalytic killing efficiency (99.94%) against airborne *E. coli*.[83] MOFs are burgeoning materials for bioaerosol photocatalytic inactivation, although their chemical and humidity stability are not good enough for long-term services.[87]

A photosensitizer (PS), also called a photocatalytic dye, absorbs a photon of light (with a wavelength that matches the absorption band of the dye), leading to the excitation of the dye.[88] PSs could generate biocidal reactive oxygen species (ROS) in polymers under light exposure, and the ROS could damage protein, DNA, and lipid of microorganisms, resulting in rapid inactivation.[89] Benzophenone, anthraquinone, and xanthene derivatives are representative photoactive compounds and have been applied in polymers and fabrics to provide rapid antibacterial functions with acceptable washability and photostability.[65,90] Tang *et al.* employed anionic photosensitizers (rose Bengal and sodium 2-anthraquinone sulfate) on cotton fibers through strong electrostatic interaction, producing biocidal ROSs under light exposure and consequently providing photo-induced biocidal functions. The treated fibers achieved a 99.9999% (6 log) reduction in bacteria and bacteriophage levels within 60 min of daylight exposure.[65] Heo *et al.* introduced a visible-light-activated antimicrobial fiber mat functionalized with TiO_2-crystal violet nanocomposites, exhibiting a potent inactivation rate of ~99.98% against various bioaerosols.[91] The dyed fibers can be applied to facemasks with bioaerosol photocatalytic inactivation to avoid secondary bioaerosol contamination. Photocatalytic dyes are easily modifiable and can be combined with various substrates and have no substrate selectivity, but they have relatively short wavelength excitation light and poor chemical stability.[73]

The photocatalytic oxidation process for bioaerosol inactivation is defined by the generation of electrons and holes through the irradiation of a photocatalyst with light. Electron transfer can lead to the production of superoxide radicals ($^{\bullet}O_2^-$) and then hydroxyl radicals ($^{\bullet}OH$), and also involves energy transfer to produce excited state singlet oxygen ($^1O_2$). Both $^{\bullet}OH$ and $^1O_2$ are highly ROSs that can damage nearly all types of biomolecules (proteins, lipids and nucleic acids) and kill cells.[92,93] As shown in Fig. 4a–d, photocatalysts including MOFs, metal oxides and their compounds, photosensitizers (dyes) and MXenes generate highly active ROSs in air to attack microbes, destroying the microbial structure and their genetic material.[94] During the photocatalytic inactivation process, it is usually necessary for bioaerosols to come in contact with the photocatalysts as ROSs cannot be remotely transported.[95]

The bandgaps of some typical semiconductors are shown in Fig. 5a. It is well known that the potential of $^{\bullet}OH$ is +2.38 V ($^{\bullet}OH/H_2O$ = +2.38 V *vs.* NHE) and $^{\bullet}O_2^-$ is −0.33 V. TiO_2 only absorbs ultraviolet light, owing to its large bandgap of 3.2 eV. As the conduction band of photocatalysts is higher than the potential of $^{\bullet}OH$, while the valence band is lower than the potential of $^{\bullet}O_2^-$, they can produce ROSs under UV light (Fig. 5b). In order to utilize visible light, the combination and doping strategies are applied to the photocatalysts. As shown in Fig. 5c and d, both Ag and CuO in metal-doped TiO_2 photocatalysts could act as intermediate agents to enhance the electron–hole separation efficiency of TiO_2.

2.2 Bio-inspired photocatalysts for bioaerosol control

Interestingly, bio-inspired photocatalysts have recently emerged as bioaerosol control methods; these photocatalysts are based on mimicking the nanostructure, chemical composition and morphology found in animals and plants in nature.[96,97] Nature has wisdom to solve problems, like enemy defense, food hunting, environment adaptation, effective movement and so on.[98,99] Researchers found that the cicada and dragonfly wings show excellent bactericidal properties towards some bacterial strains due to the special nano-scale structure of spike-like

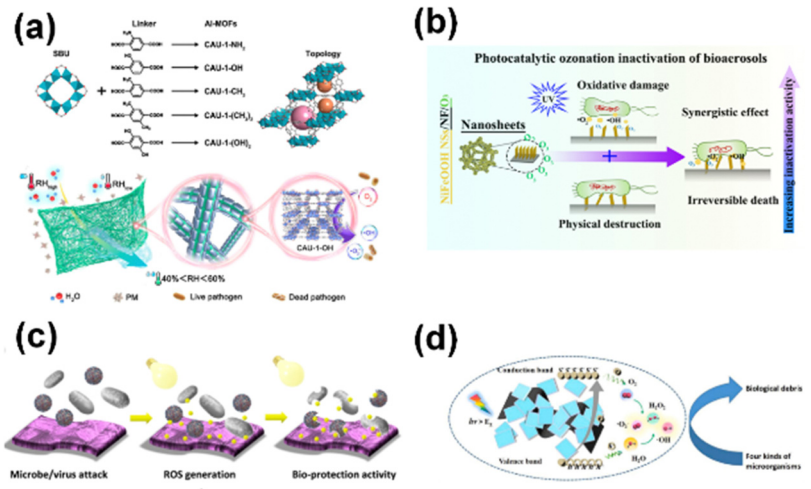

Fig. 4 Bioaerosol inactivation mechanism of photocatalysts. (a) MOF,[83] Reproduced with permission. Copyright 2020, American Chemical Society. (b) NiFeOOH nanosheets,[75] reproduced with permission. Copyright 2023, Elsevier. (c) Rose Bengal and sodium 2-anthraquinone sulfate,[65] reproduced with permission. Copyright 2020, American Chemical Society. (d) MXene, reproduced with permission.[38] Copyright 2022, Elsevier.

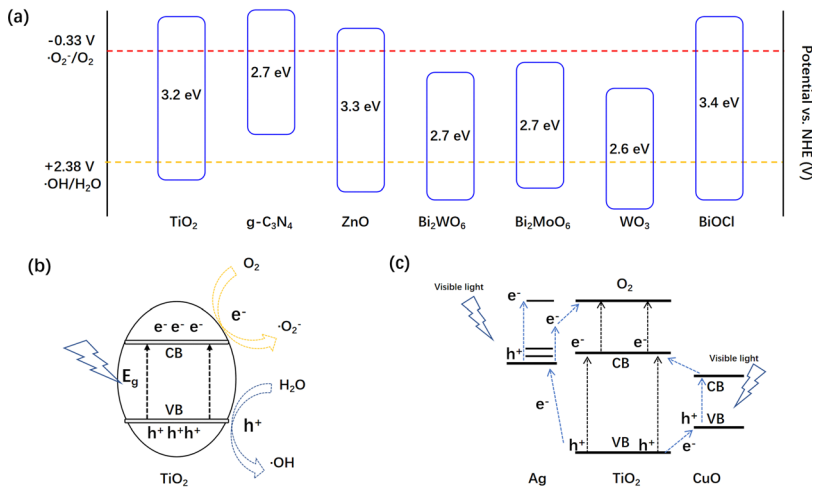

Fig. 5 The mechanism of light-induced reactive oxygen species by semiconductor photocatalysts. (a) Bandgaps of some typical semiconductors. Charge separation of (b) TiO_2. and (c) Cu and Ag doped TiO_2.

arrays. Some researchers have employed this method to fabricate homogeneous structures on photocatalysts to create micro-patterned arrays, as well as to test the influence of surface modification on bacterial adhesion in photocatalysts.[100] Recently, Wang *et al.* drew inspiration from dragonfly wings, which can inhibit, damage, and even cause the death of bacteria due to their sharp nanostructures (Fig. 6a), to introduce the concept of physical destruction caused by nanostructures into a photocatalytic oxidation (PCO) system.[75] The NiFeOOH nanosheet photocatalyst (Fig. 6b) not only offers physical destruction to destroy bacterial cell membranes, but also generates ROSs to oxidize the cell membrane. By mimicking the dragonfly wings, the NiFeOOH nanosheet photocatalyst promotes the injection of light-induced ROSs into cells, leading to fast and irreversible inactivation of airborne bacteria (Fig. 6c). Therefore, the inactivation efficiency of the PCO system was obviously improved by mimicking the structure of the dragonfly wings.

On the other hand, natural animals and plants have many smart ways to adapt to the environment. Mussels possess excellent wet adhesions to the stones as they have to adapt to strong waves in the sea.[101] In 2007, Messersmith *et al.* first reported that dopamine molecules secreted by mussels can self-assemble and adhere to any surface through intermolecular and intramolecular self-polymerization, forming polydopamine (PDA) membranes.[102] The active groups on PDA membranes, such as the catechol group, phenolic hydroxyl group, amino group, and aldehyde group, possess an affinity to biological molecules and can form hydrogen bonds and chemical bonds with biological molecules (shown in Fig. 6d).[103,104] Therefore, by mimicking mussels adhered to stones, PDA has potential applications in the "adhesive capture" of biological contaminants in bioaerosols. Peng *et al.* reported a non-size-dependent bifunctional nickel foam filter (g-C_3N_4/TiO_2(CT)/Ni-PDA/Ni bifunctional filter) with two layers of coupling nickel foams

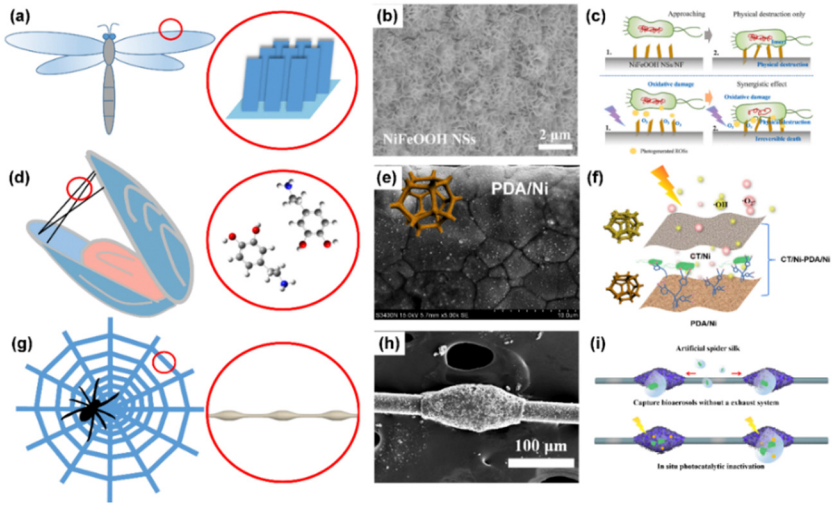

Fig. 6 Bio-inspired materials for bioaerosol control. (a) Inspired by the wings of dragonfly, (b) SEM image of the NiFeOOH nanosheets on nickel foam, and (c) mechanisms,[75] reproduced with permission. Copyright 2023, Elsevier. (d) Inspired by the secretion of mussels, (e) SEM image of the polydopamine modified nickel foam, and (f) mechanisms.[105] Reproduced with permission. Copyright 2023, Elsevier. (g) Inspired by spider silk, (h) SEM image of the artificial spider silk photocatalyst, and (i) mechanisms.[111] Reproduced with permission. Copyright 2023, Nature Publishing Group.

deposited by CT and PDA, respectively.[105] The bio-affinity of the nickel foam modified by PDA (Fig. 6e) was improved, thus significantly increasing the efficiency of bioaerosol capture despite the pore size (~200 μm) of nickel foam being much bigger than the size of bioaerosols (~1.5 μm). They used an atomic force microscope to test the adhesive forces of PDA-modified nickel foam, and discovered that adhesive force was improved by two times after PDA modification. They proposed that the bifunctional capabilities of bioaerosol capture and inactivation in the filter arise from the top CT/Ni layer of the CT/Ni-PDA/Ni filter, which generates and transports ROSs to downstream, while the bottom bio-affinity PDA/Ni layer of the CT/Ni-PDA/Ni filter capture the microorganisms in the air (Fig. 6f). The high efficiencies for bioaerosol capture and inactivation by the non-size dependent filter were achieved through inspiration drawn from mussel secretions.

In nature, spider silk can actively capture tiny dust particles and microdroplets from air; the microdroplet coalesces to form larger droplets, which concentrate small dust particles and moisture on the spider silk.[106] Jiang *et al.* reported that the water-collecting capacity of cribellate spider capture silk is the result of a unique fiber structure that consists of periodic spindle knots separated by joints (Fig. 6g).[107,108] By mimicking this special fiber structure, many researchers have developed artificial spider silk (ASS) for water collection from the air in arid regions.[109] It can be considered that airborne microorganisms mainly exist in water microdroplets, particle matter, and aggregations that are dispersed in air.[110] Recently, Peng *et al.* have designed a bioinspired ASS photocatalyst, consisting of a periodic spindle structure of TiO_2 on nylon fibers (Fig. 6h) that can efficiently capture and concentrate airborne bacteria, followed by photocatalytic inactivation *in situ*.[111] As shown in Fig. 6i, the capture capacity of the ASS photocatalyst can be mainly attributed to the synergistic effects of hydrophilicity, Laplace pressure differences caused by the size of the spindle knots and surface energy gradients induced by surface roughness. The captured microdroplets are quickly concentrated onto the spindle knots, leaving the joints as capture sites for continuous bioaerosol capture. The bacteria captured by the ASS photocatalyst are inactivated through photocatalysis within droplets or at air/photocatalyst interfaces. Therefore, the ASS photocatalyst could realize a higher bioaerosol capture and inactivation efficiency.

2.3 Other technologies combined with photocatalytic inactivation

As airborne pathogenic microorganisms are dispersed and diluted in bioaerosols, other technologies can be combined with photocatalysis to improve inactivation efficiency and to shorten the process time. The combination technologies have been extensively applied for water disinfection, while their application in bioaerosol control is rare, presented in Fig. 7. O_3 is an efficient air disinfectant, while high concentration of it is harmful to humans. However, by combining O_3 with photocatalytic technology, the concentration of O_3 can be largely reduced. As reported by

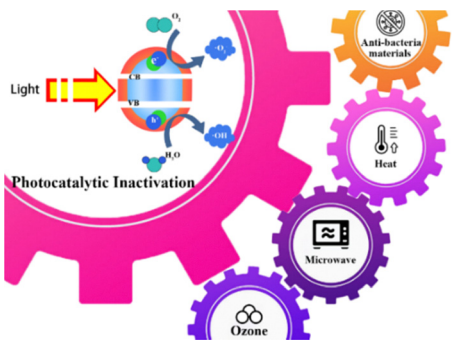

Fig. 7 Combination of photocatalytic inactivation with other technologies.

Wang *et al.*,[75] in a single photocatalytic reaction system, ROSs are generated through a H_2O_2-mediated three-electron-reduction route, resulting in a relatively low yield of ROSs, yet for the photocatalyst–O_3 system, ROSs can also be generated through an additional $^{\bullet}O_3^-$-mediated one-electron-reduction pathway.[112] Moreover, O_3 ($E(O_3)$ = 2.07 V *vs.* NHE) possesses a higher oxidation potential compared to O_2 ($E(O_2)$ = 1.23 V *vs.* NHE), making it thermodynamically easier for O_3 to capture photogenerated electrons in this process.[113] Therefore, trace O_3 significantly improves the ROS generation in the PCO system, resulting in highly-efficient inactivation performance.

Photocatalytic inactivation can also be combined with thermal treatment for irreversible mineralization of bioaerosols. At present, thermal–photocatalytic inactivation technology is used for water disinfection. The MoO_{3-x}-rGO composites with a synergistic photothermal and photocatalytic performance were prepared by the solid-phase microwave thermal shock method.[114] The super-hot spots created on the surface of microwave-reduced rGO induce the formation of MoO_{3-x} with oxygen vacancies. Due to the localized surface plasmon resonance effect, the near-infrared photothermal and photocatalytic properties of MoO_{3-x}-rGO catalysts are greatly improved. The generated holes on photocatalysts could directly inactivate bacteria or be captured by H_2O to form hydroxyl radicals with deadly effects on bacteria.[115]

Microwave irradiation has been used for bioaerosol inactivation through various mechanisms including thermal effects, disruption of weak bonds in active protein forms, enhanced production of reactive oxygen species, and cell-signaling pathway interference as bioaerosols can absorb microwaves.[116–118] Wu *et al.* investigated the survival of bioaerosols on exposure to microwave irradiation (2450 MHz) for 2 min at different output powers (700, 385 and 119 W). The survival rates of airborne *B. subtilis var. niger* spores were shown to be about 35%, 44% and 35% when exposed to microwave irradiation for only 1.5 min with high, medium and low power applied, respectively (p-value = 0.37).[119] The results indicate that microwave irradiation can be used to develop a quick microwave-based air sterilization technology, which may show better performance than water disinfection due to lower heat loss. Therefore, the combination of microwave and photocatalytic inactivation may overcome the shortcoming of the long process time of photocatalytic inactivation. However, the combination of the photocatalytic inactivation and microwave irradiation has not been reported so far.

Moreover, the photocatalytic inactivation technology is capable of inactivating bioaerosol under light irradiation, while in dark, there is no ROS generation and the function of photocatalytic inactivation fails; thus the combination of antibacterial materials provides the bactericidal capability in dark. Tang *et al.* reported that the nanopillar array of ZnO/Au on polydimethylsiloxane (PDMS-ZnO/Au) exhibited two-fold bactericidal activity. The obtained PDMS-ZnO/Au surface demonstrates physical antibacterial performance, resulting in a killing rate of 65.5% in dark. Furthermore, the surface effectively inactivates bacteria under visible light irradiation, yielding a lethality >99.9% in 30 min. The advantages of a high lethality rate and short action time are conferred upon PDMS-ZnO/Au through a two-fold antibacterial action that combines enhanced photocatalysis resulting from the introduction of Au nanoparticles and the mechanical properties of a biomimetic nanostructure.[100] The nanopillar arrays of ZnO enable physical bacteria killing both in dark and under light exposure. The incorporation of Au nanoparticles can extend the light absorption range and improve photocatalytic activities due to localized surface plasmon resonance (LSPR).

2.4 The recycling ability of the photocatalysts

Air disinfection is a continuous process as the emission of bioaerosols continues as long as when people are present. Therefore, the recycling ability of the photocatalyst should be considered for long-term service. Traditional methods of regeneration of the air filter are back-blowing, pulse-blowing, mechanical shaking, heating, solution washing and hydrophobic modification. However, the recycling ability of the photocatalysts are rarely investigated. The inactivation efficiency of the photocatalysts declines due to light blocking caused by the coverage of microbes. Therefore, the washing and heating process may be the preferred methods for recycling of photocatalysts. The heating method is suitable for thermally stable photocatalysts and carriers as it can remove the microbes completely. Therefore, some organic photocatalysts and carriers cannot withstand the harsh treatment conditions for recycling. On the other hand, washing is a mild method for recycling, but it can lead to the removal of static electricity and photocatalysts from the materials, resulting in poor removal and inactivation efficiency of bioaerosols after recycling.

3. The photocatalyst carriers and assembled photocatalytic reactors

Photocatalysts are usually in the nano- or micro-sized powdered form and cannot be directly used in bioaerosol inactivation like in water disinfection through dispersion. Porous materials are used as carriers to support photocatalysts, and then assembled in photocatalytic reactors or loaded on the other substrates for practical uses.

3.1 The carriers of photocatalysts

In order to adapt to the practical uses of bioaerosol photocatalytic inactivation, photocatalysts are usually loaded on the carriers or substrates, exposing their surfaces to the light source.[120] There are majorly four structural types of carriers as shown in Fig. 8, namely, porous structures, meshes, packed beads and fibrous membranes. Good support and mechanical properties are essentially required for porous structures with large porosity due to high air velocity in air purification systems.[121]

Self-supporting metallic and polymeric porous materials are chosen as carriers of photocatalysts for bioaerosol coarse filters. Porous nickel foam with a hole size of 200–300 μm[75] and polyurethane sponge with a pore diameter of 30 pores per inch are currently being investigated.[38,51,63,122] Photocatalysts are loaded on the surface of the skeletons exposed to light

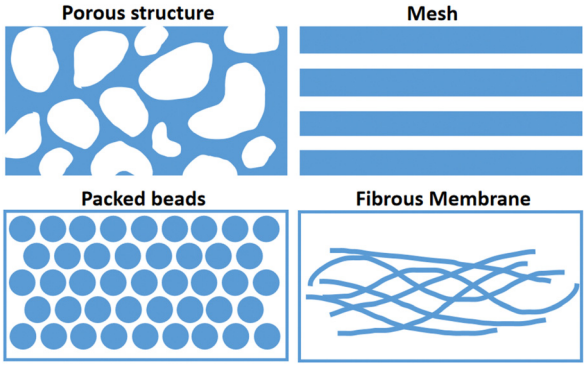

Fig. 8 The structures of photocatalyst carriers.

irradiation. In order to enhance the interaction between the photocatalysts and the bioaerosols, porous materials with large thicknesses are applied in the photo-reactor.[51] The size of these porous structures is usually much bigger than that of bioaerosols, which facilitates low-pressure drop and light penetration.[123] However, upon being captured by three-dimensional porous materials, microorganisms usually enter the pores of these materials due to weak interactions between the microorganisms and materials. Light penetration is inhibited in the deep pores of materials; thus, photocatalytic inactivation efficiency decreases.

Metallic meshes are frequently used in commercial air purifiers as coarse filters.[32,34,124] As photocatalysts carriers, stainless meshes were coated with ZnO photocatalysts through the painting method for bioaerosol photocatalytic inactivation.[125] The pore size of two-dimensional-sheet meshes is even larger than 500 μm, allowing light transmission and avoiding blockage.[126] The drawback of the mesh carrier is that the thin thickness of the mesh reduces the interaction between the bioaerosols and photocatalysts, yielding low inactivation efficiency.

Millimetre beads modified with photocatalysts can be packed in the photoreactor as carriers for bioaerosol inactivation. Hydrogel beads,[127] ceramic beads[128,129] and glass beads[55,92] are currently modified with photocatalysts and applied to a continuous flow reactor. Photocatalysts are modified on/in the beads through surface coating, mixing and painting.[92] Air streams pass through the gaps between the beads, while airborne microorganisms are intercepted by beads for photocatalytic inactivation.[20] Smaller-sized beads lead to lower porosity in the reactor due to dense packing. Photocatalyst-modified beads can be easily prepared for mass production. At the same time, they have the advantage of easy replacement. However, large pressure-drop, low light penetration, and easy blocking limit their application.

Last but not the least, fibrous membranes as a carrier of photocatalysts have been intensively investigated. Fibers with diameters in the nanometre or micrometre range, like polypropylene (PP), polyethylene (PE), polyester (PET), polyamide (PA) and polyacrylonitrile (PAN), are commonly used as nonwoven fibrous mats.[130,131] Photocatalysts can be loaded on nonwoven fabrics by spray coating,[91] hot-press approaches,[64] dip coating,[83,85] dyeing processes[65] and electrospinning.[86,132] Fibrous membranes as photocatalyst carriers can be used as facemasks, clothes, and filters for bioaerosol photocatalytic inactivation, possessing advantages of big surface area, easy preparation, high porosity, flexibility, low pressure-drop and high efficiency.[64,65,91] At the same time, they also have shortcomings such as lack of self-support, poor fastness, and susceptibility to blocking.[133,134]

The types, loading methods, carriers and removal efficiency of photocatalysts in various photocatalytic inactivation systems are summarized in Table 1. It can be seen that the fibrous carriers generally offer higher removal efficiency for bioaerosols compared to the beads. However, the evaluations of removal efficiency are different, and the results are cursory.

In addition, the bioaerosol photocatalytic inactivation efficiency varies when dealing with different types of bioaerosols. Gram-negative bacteria show better tolerance to photocatalytic ROSs than Gram-positive bacteria because they have a complex cell wall and an additional outer membrane composed of lipopolysaccharides, which protect them from the attack of ROSs to a certain extent.[22] Therefore, microbes with different chemical structures show different levels of resistance to photocatalytic inactivation.

3.2 The reactors of photocatalyst

The photocatalysts were usually loaded in a photocatalytic reactor for bioaerosol inactivation. As shown in Fig. 9, there are usually four types of reactors including fixed bed, array, fluidized bed and cyclone, which have their origins in industrial dust removal reactors. The photocatalysts are first loaded on the carriers and then assembled in the reactors, equipped with light sources. The diagram of a fixed bed reactor is shown in Fig. 9a; the photocatalysts are assembled at the middle of the reactor, perpendicular to the direction of the inlet air flow. The bioaerosols pass through the photocatalysts, where they are intercepted by the photocatalysts and inactivated. In this situation, the airflow has to pass through the porous photocatalyst carriers, leading to high removal efficiency but high pressure-drop and easy blocking. In the array type reactor as shown in Fig. 9b, several photocatalytic carriers are assembled in parallel along the direction of the inlet air flow. The bioaerosols go along with the photocatalytic carriers, yielding low pressure-drop and long contact distance. However, as the bioaerosol does not pass through the photocatalysts, removal efficiency of this kind of reactor is relatively low. A fluidized bed reactor (Fig. 9c) is a kind of reactor where the inlet direction of bioaerosols is opposite to the gravity direction. The photocatalysts are loosely suspended and move along with the air flow in the reactor. In this reactor, bioaerosols can come in full contact with the photocatalysts. The photocatalysts are blown by the air flow and fall down due to gravity. The light utilization of this reactor is insufficient as the light cannot penetrate deep into photocatalysts. The pressure-drop and removal efficiency are dependent on the amount of photocatalysts. The cyclone type reactor is based on centrifugal forces for separating the airborne microorganisms from the airflow (Fig. 9d). The bioaerosols go along with the helical track and may deposit on the photocatalyst. In this situation, the airflow is also parallel to the

Table 1 Types, loading modes, carriers and removal efficiency of photocatalysts in photocatalytic inactivation systems

Photocatalysts	Loading method	Carrier	Microorganism	Removal efficiency (%)	Ref.
TiO_2	Dip coating process	Glass	*B. subtilis*	100	135
		Reactor inner wall	*Legionella pneumophila*	94	136
		High efficiency particle air filter cartridge	*E. coli*	100	137
		—	Various bacteria and fungi	77	138
		—	*S. epidermidis, B. subtilis, Aspergillus niger, Penicillium citrinum*	98	139
		Polyether sulfone disc filter	*E. coli*, *B. subtilis*, microbacillus	100	140
		Borosilicate plate	Various bacteria and fungi	98	141
		Glass fiber filter	*E. coli* K-12	100	142
		β-SiC foam	T2 bacteriophage	99.9	143
		Porous ceramic	H1N1 virus	100	144
		Aluminum plate	H1N1 virus	99.999	145
		Ceramic foam	*E. coli*, *Pseudomonas aeruginosa, Klebsiella pneumoniae, L. pneumophila*, methicillin-resistant *S. aureus* (MRSA)	99.9	146
	Sol–gel method	Glass fiber	MRSA	97.7	147
	Chemical grafting	Polyurethane foam	*L. pneumophila*	90	148
TiO_2 or ZnO	Dip coating process	Cellulose acetate honeycomb structure	Various bacteria and fungi	98	149
		Poraver glass beads	Bacteria and fungi	78	150
	Sol–gel method	Perlite, Poraver glass beads	Bacteria and fungi	77	151
		Perlite	Bacteria and fungi	70	56
Cu/TiO_2	Sol–gel method	Glass fiber	*E. coli*	87.80	152
		Non-woven fabric	Human norovirus	99.87	153
	Chemical grafting	Polyurethane foam	*Candida famata*	—	154
Ag/TiO_2	Dip coating process	Fabric filter	Bacteria, fungi, viruses	100	50
		Aluminum plate, Polyester fiber	*B. cereus* spores	97.89	155
Cu/TiO_2, Ag/TiO_2	Sol–gel method	Glass fiber	*E. coli, Staphylococcus aureus*	94.46	156
TiO_2/Cu^{2+}, $Ag@TiO_2/Cu^{2+}$	Dip coating process	Perlite	*E. coli*, *S. aureus*	100	157
Pd/TiO_2	Electrostatic self-assembly method, Sol–gel method	Titanium plate	MS2 bacteriophage	100	52
TiO_2, Pt/TiO_2	Dip coating process	Glass plate	Various bacteria and fungi	99.8	158
Ag/TiO_2, Ag/ZnO	Spraying method	Reaction lamp inner surface	Ambient air bacteria	96.48	159
ZIF-8	Hot pressing	Non-woven fabric	*E. coli*	99.99	64
TiO_2/MXene	Dip coating process	Polyurethane foam	*E. coli*	99.96	160
TiO_2/MXene	Dip coating process	Polyurethane foam	Multiple *E. coli*	99.99	161
TiO_2/MXene	Dip coating process	Polyurethane foam	*E. coli*, *S. aureus, Aspergillus versicolor* spore, MS2 phage	6.22 lg	162
CT/Ni-PDA/Ni	Hydrothermal-calcination approach and electrophoresis technique	Ni foam	*E. coli* K-12	93.5	105
NiFeOOH NSs	Hydrothermal process	Nickel foam	*E. coli* K-12	99.99	75
TiO_2/PMMA spindle knots (artificial spider silk)	Dip coating process	Nylon fibers	*E. coli* K-12	99.99	111

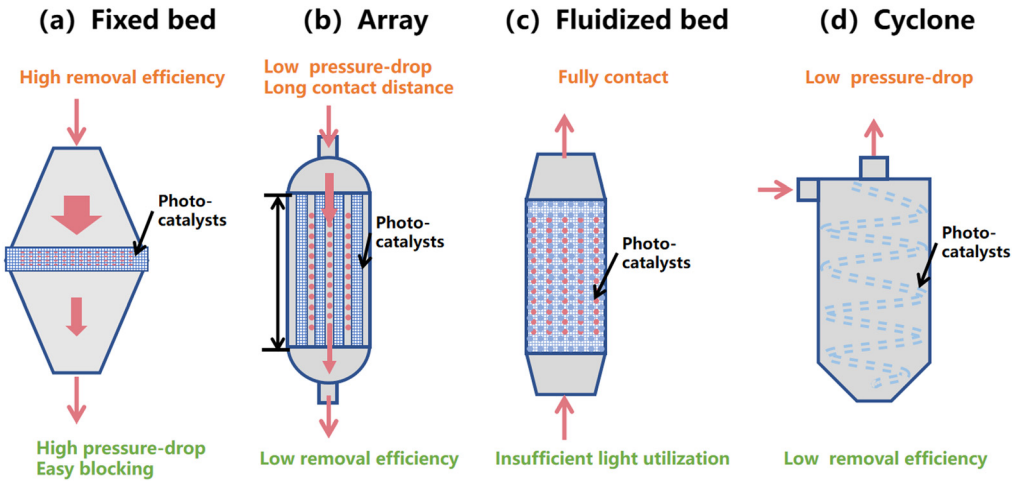

Fig. 9 Assembled photocatalytic reactors of photocatalysts. (a) Fixed bed, (b) array, (c) fluidized bed, and (d) cyclone.

plane of the photocatalysts, yielding relatively low pressure-drop and removal efficiency.

3.3 The light sources of photocatalysts

The light sources assembled in photocatalytic reactors are varied due to different photocatalyst loadings, yielding different light utilizations. As shown in Fig. 10, the light sources can be placed on the top, side and at the middle of the reactor, as well as in arrays and annular types. The light sources placed on the top, side and middle of the reactor are usually found in relatively simple photocatalytic inactivation systems. The photocatalysts are irradiated in a single plane, which is suitable for fixed bed reactors where bioaerosols pass through the photocatalysts. Their disadvantages are uneven illumination and low light intensity. On the other hand, array and annular assembled light sources can provide multi-angle irradiation to photocatalysts and are found in relatively complicated and energy consuming reactors like arrays and cyclone types for sufficient, uniform, and multi-angle irradiation.

The removal efficiency, light source position and reaction time of reactors in photocatalytic inactivation systems are summarized in Table 2. The structure of the reactor, light positions and the microorganisms as well as the reaction times are varied in different studies. The reaction time of photocatalytic inactivation ranges from seconds to hours as different performance evaluations.

The wavelengths of light sources are usually dependent on the photocatalysts. The photocatalysts that respond to UV light, like TiO_2, ZnO, NiFeOOH and so on[55,168] are shown in Fig. 11a. The reactor is made of quartz which is transparent to UV light if the light source is placed outside of the reactor, thus reducing the light loss. UV photons are quite high in energy,[169] and photocatalysts can be easily excited by the UV light, generating ROSs for bioaerosol inactivation. Direct irradiation with UV light, however, results in substantial photodecomposition of the carriers and is harmful to humans. Visible light is a potential candidate for photocatalytic inactivation technology as presented in Fig. 11b. The use of visible light which is most strongly emitted in the solar spectrum in photocatalytic inactivation is challenging because visible light photons possess relatively low energy to excite photocatalysts, leading to lower ROSs generation. Therefore, these kinds of photocatalysts utilize UV and visible light at the same time, including TiO_2/CdS, TiO_2/CuO,[66] g-C_3N_4/TiO_2,[105] and dyes.[91]

Indeed, infrared light occupies the largest proportion in the solar spectrum, and the absorption of near-infrared light can also excite the photocatalyst for bacterial inactivation in water,

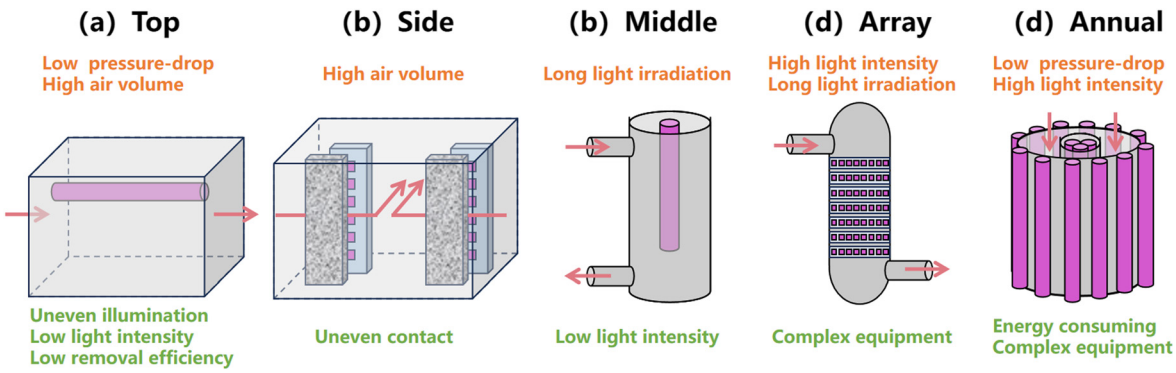

Fig. 10 The assembled light sources in the reactor: (a) top, (b) side, (c) middle, (d) array and (e) annular.

Table 2 Light source position, removal efficiency and reaction time of reactors in photocatalytic inactivation systems

Light source position	Microorganism	Reaction time	Removal efficiency (%)	Ref.
Top	Bacteria	48 h	96.48	159
	E. coli	4 h	100	137
	E. coli K-12	8.07 s	99.99	75
	Microorganism	300 min	100	163
	Bacteria	48 h	96.48	159
Side	Bacteria, fungi, viruses	2 min	100	50
	Bacterial, and fugal	4.3 s	83.6	164
	H1N1 virus	7 min	99.999	145
Middle	Various bacteria and fungi	8 h	77	138
	Bacteria, fungi	5.7 s	77	151
	E. coli	4.27 s	99.96	160
	Multiple *E. coli*	4.27 s	99.99	161
	Various bacteria and fungi	0.3 min	98	149
	E. coli K-12	1.1 min	100	142
	E. coli	—	97.7	147
	L. pneumophila	1.5 s	90	148
	MS2 bacteriophage	0.125 s	100	52
	L. pneumophila	—	94	136
Array	Bacteria	6 s	99.9	165
	E. coli	1 h	87.80	152
	T2 bacteriophage	60 min	99.9	143
	E. coli	1 h	100	157
	B. subtilis var. niger	0.21 s	93.1	166
	Enterococcus faecalis, bursal disease virus	1 h	99.7	167
	E. coli, *P. aeruginosa*, *K. pneumoniae*, *L. pneumophila*, MRSA	24 h	99.9	146
	H1N1 virus	5 min	100	144
Annular	*B. subtilis* (vegetative cells and spores)	60 min	100	135
	E. coli, *B. subtilis*, microbacillus	3.57 min	100	140

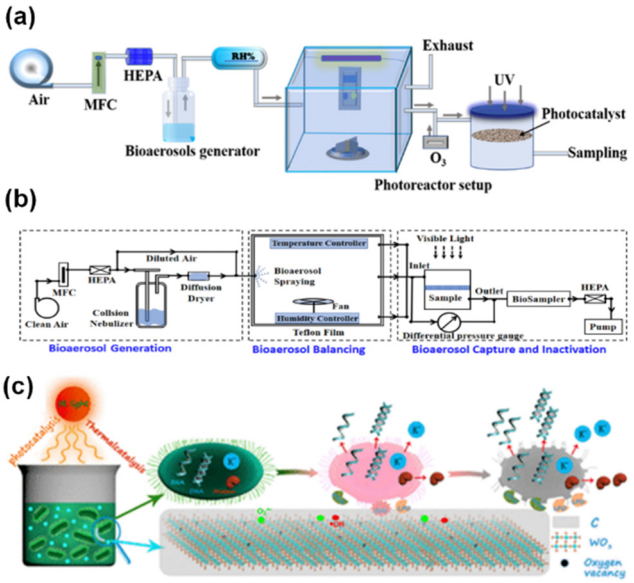

Fig. 11 The wavelength utilized by photocatalysts. (a) UV,[75] reproduced with permission. Copyright 2023, Elsevier. (b) Visible light,[105] reproduced with permission. Copyright 2023, Elsevier. (c) Infrared,[171] Reproduced with permission. Copyright 2020, American Chemical Society.

so it is of great significance to utilize infrared light for bioaerosol inactivation.[170] Zhang *et al.*[171] reported tungsten trioxide with coexisting oxygen vacancies and carbon coating (WO_{3-x}/C) for photothermal inactivation of *E. coli* (Fig. 11c). Oxygen vacancies and carbon coating cause WO_{3-x}/C strong absorption in the infrared region and enhance the carrier separation efficiency, leading to complete inactivation of *E. coli* under infrared light within 40 min. However, infrared used in bioaerosol inactivation has not been reported yet, while it may show potential as it is abundant and safe for humans.

The wavelength and intensity of light sources in photocatalytic inactivation systems are summarized in Table 3. It can be seen that UV light is the most used radiation in photocatalytic inactivation with relatively low power. Visible light and simulated sunlight are less studied, while infrared has never been reported in photocatalytic inactivation of bioaerosols.

4. Practical applications and performance evaluation

Photocatalysts loaded on different carriers and assembled in different photocatalytic reactors can be applied to different applications for bioaerosol inactivation. As shown in Fig. 12, photocatalysts can be applied to air cleaners, windows, walls, facemasks, and clothes for bioaerosol inactivation by using solar and artificial lights.[48,64,65,74] The photocatalytic technology can inactivate the bioaerosols when human activity is present, and airborne microorganisms are continuously produced.[53,69] Photocatalysts loaded on porous structures, meshes and packed

Table 3 The wavelength and intensity of light sources in photocatalytic inactivation systems

Light source	Power	Light intensity ($mW \cdot cm^{-2}$)	Microorganism	Removal efficiency (%)	Ref.
UVA	6 W × 19	Inner side: 3.43; outer side: 1.89	*B. subtilis*	100	135
	8 W × 2	1.82–6.28	*E. coli*, *B. subtilis*, microbacillus	100	140
	14 W × 6	10	Bacteria, fungi, viruses	100	50
	14 W × 43	5	*B. cereus* spores	97.89	155
	36 W × 5	4.85 ± 0.09	Various of bacteria and fungi	77	138
	8 W × 2	0.5–3.4	*E. coli* K-12	100	142
	—	1	H1N1 virus	100	144
	—	0.25	*E. coli*, *P. aeruginosa*, *K. pneumoniae*, *L. pneumophila*, MRSA	99.9	146
UVC	—	1.8	*S. aureus*	99.98	172
	18 W, 35 W	0.06–0.105	Various pathogenic bacteria and viruses	99.99	173
	11 W × 2	12.8	*E. faecalis*, bursal disease virus	99.7	167
UVC	15 W	10	*E. coli*	99.96	160
UVA	8 W	10	*E. coli*	99.68	
UVC	6 W	1.4 ± 0.09	*S. epidermidis, B. subtilis, A. niger*,	87	139
UVA	6 W	2.2 ± 0.06	*Penicillium citrinum*	73	
VUV	0.5–11 W	—	MS2 bacteriophage	100	52
UV (185 + 254 nm)	55 W × 2 or 80 W × 2	0.2	*B. subtilis var. niger*	93.1	166
UV-LED (392 nm)	0.0097 W × 56	11.7 ± 2.0	T2 bacteriophage	99.9	143
UV-LED (375 nm)	2 W × 12	—	H1N1 virus	99.999	145
UV-LED (365 nm)	20 W	—	*E. coli* K-12	99.99	75
UVA (365 nm)	—	12	*E. coli* K-12	99.99	111
UV (185–254 nm)	—	—	Bacteria and fungi	83.6	164
UVA (365 nm) and UVC (254 nm)	8 W/16 W/23 W	40.5/92.2/66.8/ 88.6/135.3	Multiple *E. coli*	99.99	161
Blue-LED (430–505 nm) UV-LED (380–420 nm)	(30 mA, 3.6 V) × 60 (500–700 mA, 3.2–3.6 V) × 6	—	*E. coli*, *S. aureus*	100	157
Blue-LED (420 nm)	6.8 W × 85	—	Bacteria	99.9	165
Visible light (405 nm)	7 W	—	Bacteria	96.48	159
Visible light	20 W × 4	25	*E. coli*	87.80	152
	20 W × 4	25	*E. coli*, *S. aureus*	94.46	156
Simulated sunlight (300–1100 nm)	300 W	100	*E. coli*	99.99	64
Visible light		400	*E. coli* K-12	93.5	105
Sunlight	—	18–21	*S. epidermidis*	99.98	91

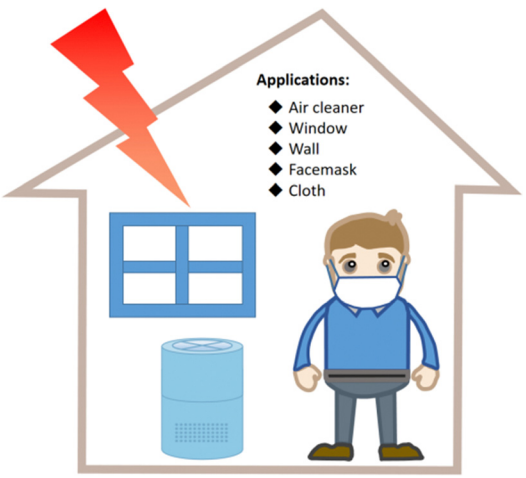

Fig. 12 Applications of photocatalysts in bioaerosol control.

beads are more frequently applied to air cleaners with high treatment capacity for large volume of air that can be efficiently treated per minute. The air cleaner with photocatalytic inactivation technology is able to handle high concentration of bioaerosols in a short time.[75] Windows, walls, facemasks, and clothes fail to provide power for bioaerosol flow, resulting in the passive deposition of airborne microorganisms on their surfaces. Their treatment capacity is limited but can still effectively prevent bioaerosol secondary contaminations.

Wide-range applications of bioaerosol photocatalytic inactivation led to various performance evaluation methods, which can be classified into performance evaluations of bioaerosol capture and inactivation. For evaluating the bioaerosol capture performance of the filter, the goal is to evaluate the number of airborne microorganisms reduced in air by the filter treatment. While for evaluating the bioaerosol inactivation performance of the filter, the activity of airborne or captured microorganisms was characterized.

There are two main ways to assess the bioaerosol capture performance of the filter, including blowing and pumping bioaerosol for separating airborne microorganisms from the bioaerosol air flow (Fig. 13). In the former method, bioaerosols are passed through the filter as shown in Fig. 13a for comparing the number of airborne microorganisms of polluted room (left) and clean room (right) to evaluate the bioaerosol capture performance.[64] In this method, the airborne microorganisms

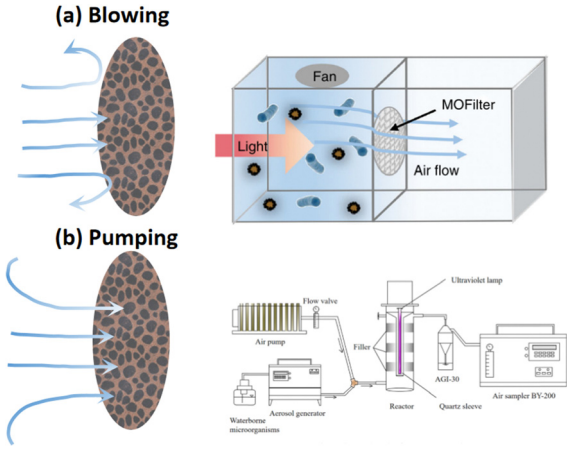

Fig. 13 Performance evaluations of bioaerosol capture. (a) Bioaerosol blowing,[64] reproduced with permission. Copyright 2019, Nature Publishing Group. (b) Bioaerosol pumping,[38] reproduced with permission. Copyright 2022, Elsevier.

are injected and dispersed in the polluted room with a fan, and a photocatalysts filter is placed between the polluted room and the clean room. The airborne microorganisms of bioaerosols are blown and trapped on the surface of the filter, clean air is injected in the clean room. In this blowing mode, with the increase in velocity of the blowing air flow rate, the capture efficiency may be increased due to more airborne microorganisms being trapped on the surface of the filter. However, the high positive pressure in the clean room will hinder bioaerosols from entering and depositing in the polluted room, resulting in the capture of fewer airborne microorganisms by the filter and higher efficiency of decreasing bioaerosols. Thus, the ratio of the number of airborne microorganisms in the clean room to that in the polluted room cannot reflect the actual capture performance of the filter. This blowing mode is more suitable for evaluating the capture performance of windows, walls and other surfaces of the filter with low-pressure drop.

On the other hand, as shown in Fig. 13b, the bioaerosols were continuously generated and pumped going through the filter.[38] By comparing the number of airborne microorganisms with and without a filter to evaluate the capture performance of the filter. In this method, the flow of bioaerosol generation and pumping remains the same; thus the airborne microorganisms are continuously generated and filtered. The exhaust of the filtered air flow is collected directly using a bioaerosol sampler at the outlet of the system.[63] The airborne microorganisms may deeply go into or penetrate the filter along with the air flow, and intercepted by the filter and separated from the air flow. This evaluation system mimics the situation of the human occupied room with continuously production of bioaerosols, while the air purifier continuously pumped and filtered the bioaerosols. Due to the drag force of the air flow, the airborne microorganisms penetrate the filter more easily compared to the blow mode,[174] leading to the capture of fewer airborne microorganisms by the filter and lower efficiency of decreasing bioaerosols. In other words, it means that in this evaluation system, the capture efficiency of the filter will decrease when the velocity of air flow is increased. However, this pumping mode restricts the air flow rate of filtration due to the limitation of the air flow rate of the bioaerosol sampler. Too high or low velocity of the flow rate may reduce the collection efficiency of the bioaerosol sampler, resulting in lower capture efficiency of the filter. Thus, this pumping mode is suitable for evaluating continuous filtrations with a relatively slow air flow rate.

In the case of two evaluation modes of capture performance, the evaluations of inactivation performance are correspondingly classified into intermittent and continuous types (Fig. 14). In the intermittent type, the evaluations of bioaerosols capture and inactivation are separated.[64] The sample filter is loaded with microorganisms through spray loading and droplet loading before being illuminated by the light source for a period of time (Fig. 14a and b). By spraying airborne microorganisms on the sample filter, the microorganisms are more dispersed and with less water, which is close to the real bioaerosols. On the contrast, the microorganisms are more concentrated by droplet loading with large amount of water, yielding difficulty in wetting hydrophobic surfaces.[65,175] In order to characterize the inactivation efficiency, the microorganisms are eluted from the sample filter for counting after photocatalysis. In this situation, the microorganisms captured by the filter would be

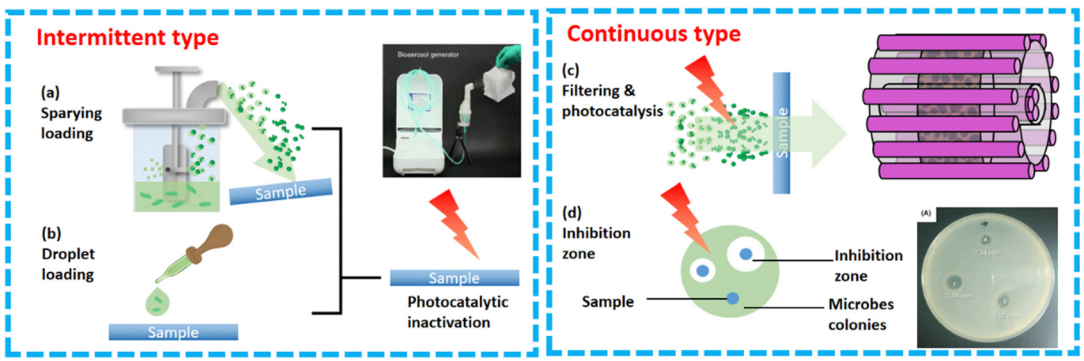

Fig. 14 Performance evaluations of bioaerosol inactivation. (a) Spraying loading with following irradiation.[64] Reproduced with permission. Copyright 2019, Nature Publishing Group. (b) Droplet loading with the following irradiation. (c) Filtering and photocatalysis. (d) Inhibition zone.[127] Reproduced with permission. Copyright 2019, Wiley-VCH GmbH.

inactivated due to photocatalysis and dehydration.[176] The microorganisms can be inactivated completely by prolonging the irradiation time. Thus, the resulting photocatalytic inactivation efficiency is high, usually reaching 99.9999%.[64] This method is more suitable to evaluate the photocatalytic inactivation efficiency of the facemask, membrane, wall, and clothes.

On the other hand, in the continuous type, the evaluations of bioaerosols capture and inactivation are simultaneous. As shown in Fig. 14c, in a continuous photocatalytic inactivation system, the bioaerosols are filtered and inactivated by photocatalysis at the same time.[74] Fresh airborne microorganisms are consecutively trapped in the filter. Therefore, the inactivation efficiency is not as high as the intermittent type if without additional irradiation. The inactivation efficiency of this method is related to the retention and filtration time. With prolonged retention and filtration time, the interaction time between the microorganisms and photocatalyst increases, leading to a rise in inactivation efficiency. The bioaerosol inactivation system should have a low airflow rate for a large mass transfer, which contradicts the large volume of treatment capacity.[123] Therefore, balance between inactivation efficiency and bioaerosol treatment capacity should be considered. The other method shown in Fig. 14d is inhibition zone under light irradiation.[127] In this situation, photocatalytic inactivation and growth of the microorganisms are going on at the same time; the microorganisms near the photocatalysts are inactivated, and thus an inhibition zone is formed around the photocatalysts. Actually, this method cannot quantitatively reflect the inactivation efficiency of the sample, which is a simple way to demonstrate the capability of inactivation of the sample. In one word, this continuous type of bioaerosol inactivation is suitable for evaluating the continuous photocatalytic reaction system, obtaining a relatively low inactivation efficiency.

5. Summary and perspective

Due to the global epidemic of COVID-19, there has been an increased concern about airborne microorganisms, leading to increased attention on bioaerosol inactivation as a means to reduce human health risks. A variety of air cleaning technologies have been developed and even applied to commercial products. Meanwhile, bioaerosol photocatalytic inactivation technology has been intensively investigated, owing to its high efficiency and environmental friendliness. Therefore, the materials, carriers and reactors, combination with other technologies, applications and performance evaluations of photocatalytic inactivation technologies are summarized, which could provide specific understandings and directions for our research and practical applications on bioaerosol inactivation.

By designing chemical structures, morphologies and compositions of metallic oxides, MOFs, MXenes, photosensitive dyes and so on, advanced photocatalytic materials have been developed and assembled for bioaerosol inactivation. In particular, bio-inspired photocatalytic materials were recently designed to improve the efficiency of photocatalytic inactivation by mimicking the morphology of dragonfly wings, the chemical composition of mussels and the spindle structure of spider silk. The design of photocatalyst carriers and photocatalytic reactors is also very important, because they influence the interception of airborne microorganisms with photocatalysts, light irradiation, and retention time. Porous structures, meshes, packed beads and fibrous membranes are the majorly used photocatalytic carriers, with fixed bed, array, fluidized bed and cyclone types of reactors. In addition, the light sources can be assembled on the top, side, middle, annular and array configurations in the reactors; meanwhile UV, visible and infrared light can be used to excite photocatalysts for generating ROSs. Based on the above designs, the photocatalysts can not only be used in reactors for air disinfection, but can also be applied in different practical fields, like air cleaners, clothes, facemasks, walls and windows. However, due to the wide range of applications of bioaerosol photocatalytic inactivation, the evaluations of capture and inactivation performance evaluations in these systems vary, making it difficult to compare the performance of the systems. Therefore, this review clarifies the full-chain of the materials, carriers and reactors, applications and performance evaluations of bioaerosol photocatalytic inactivation technology, which may help in its development in the future study.

From what has been discussed in this review, we know that the photocatalytic inactivation technology of bioaerosols has been rapidly developed. The development of novel materials and reactors with high photocatalytic performance is a key way to enhance the bioaerosol inactivation, improve treating capacity and reduce energy consumption. This technology is young and still growing; thus, still there are some aspects that should be improved and need to be investigated further:

1. With an increase in research on nanomaterials, more and more photocatalysts including quantum dots,[177] graphite carbon nitride,[178] MOFs,[87] covalent organic framework (COFs),[179,180] Mxenes,[181,182] and $ZnIn_2S_4$-based heterostructured photocatalysts[183] can be involved in photocatalytic inactivation. Currently, bio-affinity and bio-inspired photocatalytic materials are a very promising direction. Moreover, there is an urgent need to develop reusable and renewable photocatalysts to address the issues of resource waste, long-term services and environmental contamination.

2. The capture performance of the photocatalysts restricts the inactivation performance due to limited interaction between airborne microorganisms and photocatalysts. Light penetration and mineralization of microorganisms also hinder the practical application of bioaerosol photocatalytic inactivation. The photocatalyst carriers and reactors are necessarily improved to solve the above problems. In addition, in the present state of the study, UV light is the most commonly used light source, while future research should dive into the utilization of visible and infrared light for photocatalytic inactivation of bioaerosols.

3. The future research should consider the development of coupling technologies with photocatalysts for quick bioaerosol inactivation or even mineralization, like electrostatic filtration, plasma, electroporation and air ionization to broaden the applications of the photocatalytic inactivation technology.

4. As the applications of the photocatalytic inactivation are varied, the performance evaluations are different from each

other. In order to compare and accurately evaluate the bioaerosol capture and inactivation performance of the different photocatalytic systems, unified and advanced performance evaluations are also required.

From this review, it is clear that there are some creative approaches for materials synthesis and structure design that can boost the bioaerosol inactivation performance of photocatalytic systems. Researchers should analyze specific applications, and judge the dominant factor in photocatalytic inactivation. With the advancements highlighted here and a large number of ongoing research efforts in this area, photocatalytic inactivation technology will see a big breakthrough.

Conflicts of interest

The authors declare that they have no known competing financial interests or personal relationships that could have appeared to influence the work reported in this paper.

Acknowledgements

This work was supported by the National Natural Science Foundation of China (U1901210 and 42207112), the Science and Technology Project of Guangdong Province, China (2021A0505030070 and 2022A1515010538), the Local Innovative and Research Teams Project of Guangdong Pearl River Talents Program (2017BT01Z032), and the China Postdoctoral Science Foundation (2022M710822).

Notes and references

1 M. Yao, *J. Aerosol Sci.*, 2018, **115**, 108–112.
2 W. Xie, Y. Li, W. Bai, J. Hou, T. Ma, X. Zeng, L. Zhang and T. An, *Front. Env. Sci. Eng.*, 2021, **15**(3), 44.
3 C. Cao, W. Jiang, B. Wang, J. Fang, J. Lang, G. Tian, J. Jiang and T. F. Zhu, *Environ. Sci. Technol.*, 2014, **48**(3), 1499–1507.
4 J. W. Tang, L. C. Marr, Y. Li and S. J. Dancer, *BMJ*, 2021, **373**, n913.
5 T. Santl-Temkiv, P. Amato, E. O. Casamayor, P. K. H. Lee and S. B. Pointing, *FEMS Microbiol. Rev.*, 2022, **46**(4), 1–18.
6 S. Zhang, Z. Liang, X. Wang, Z. Ye, G. Li and T. An, *Environ. Int.*, 2023, **172**, 107778.
7 C. C. Wang, K. A. Prather, J. Sznitman, J. L. Jimenez, S. S. Lakdawala, Z. Tufekci and L. C. Marr, *Science*, 2021, **373**, 981.
8 C. Jiayu, R. Qiaoqiao, C. Feilong, L. Chen, W. Jiguo, W. Zhendong, C. Lingyun, R. Liu and Z. Guoxia, *J. Environ. Sci. Public Hea*, 2019, **03**(03), 347–357.
9 Z. Xu, Y. Wu, F. Shen, Q. Chen, M. Tan and M. Yao, *Aerosol Sci. Tech.*, 2011, **45**(11), 1337–1349.
10 K. H. Kim, E. Kabir and S. A. Jahan, *J. Environ. Sci.*, 2017, **67**, 23–35.
11 S. S. Zhou, S. Lukula, C. Chiossone, R. W. Nims, D. B. Suchmann and M. K. Ijaz, *J. Thorac. Dis.*, 2018, **10**(3), 2059–2069.
12 S. M. Walser, D. G. Gerstner, B. Brenner, J. Bunger, T. Eikmann, B. Janssen, S. Kolb, A. Kolk, D. Nowak, M. Raulf, H. Sagunski, N. Sedlmaier, R. Suchenwirth, G. Wiesmuller, K. M. Wollin, I. Tesseraux and C. E. Herr, *Int. J. Hyg. Environ. Health*, 2015, **218**(7), 577–589.
13 Q. Wang, J. Gu and T. An, *Build. Environ.*, 2022, **219**, 109224.
14 F. Zhou, M. Niu, Y. Zheng, Y. Sun, Y. Wu, T. Zhu and F. Shen, *J. Aerosol Sci.*, 2021, **156**, 105798.
15 Z. Liang, Y. Yu, Z. Ye, G. Li, W. Wang and T. An, *Environ. Int.*, 2020, **143**, 105934.
16 L. Song, J. Zhou, C. Wang, G. Meng, Y. Li, M. Jarin, Z. Wu and X. Xie, *J. Hazard. Mater.*, 2022, **424**, 127429.
17 N. Zhang, P. T. Jack Chan, W. Jia, C. H. Dung, P. Zhao, H. Lei, B. Su, P. Xue, W. Zhang, J. Xie and Y. Li, *Environ. Int.*, 2021, **156**, 106723.
18 K. J. Heo, H. S. Ko, S. B. Jeong, S. B. Kim and J. H. Jung, *Nano Lett.*, 2021, **21**(2), 1017–1024.
19 B. U. Lee, *Aerosol Air Qual. Res.*, 2011, **11**(7), 921–927.
20 X. R. Hu, M. F. Han, C. Wang, N. Y. Yang, Y. C. Wang, E. H. Duan, H. C. Hsi and J. G. Deng, *Chemosphere*, 2020, **253**, 126737.
21 J. Wang, Y. Zhang, L. Kuang, J. Yang, C. Xu, B. Mu, J. Li, P. Lu, W. Song, W. Wang, A. Wu, X. Liang and J. Zhang, *Chem. Eng. J.*, 2021, **424**, 130320.
22 K. Skowron, K. Grudlewska, J. Kwiecinska-Pirog, G. Gryn, M. Srutek and E. Gospodarek-Komkowska, *Sci. Total Environ*, 2018, **610–611**, 111–120.
23 M. Buonanno, D. Welch, I. Shuryak and D. J. Brenner, *Sci. Rep.*, 2020, **10**(1), 10285.
24 S. A. Grinshpun, A. Adhikari, C. Li, T. Reponen, M. Yermakov, M. Schoenitz, E. Dreizin, M. Trunov and S. Mohan, *J. Aerosol Sci.*, 2010, **41**(4), 352–363.
25 C. Wang, X. Hu and Z. Zhang, *J. Aerosol Sci.*, 2019, **137**, 105437.
26 S. Yang, Y. C. Huang, C. H. Luo, Y. C. Lin, J. W. Huang, C. P. J. Chuang, C. J. Chen, W. Fang and C. Y. Chuang, *Clean – Soil Air Water*, 2011, **39**(3), 201–205.
27 K. G. Kostov, V. Rocha, C. Y. Koga-Ito, B. M. Matos, M. A. Algatti, R. Y. Honda, M. E. Kayama and R. P. Mota, *Surf. Coat. Tech.*, 2010, **204**(18–19), 2954–2959.
28 K. Skowron, K. Grudlewska-Buda, S. Kożuszko, N. Wiktorczyk, K. J. Skowron, A. Mikucka, Z. Bernaciak and E. Gospodarek-Komkowska, *Atmosphere*, 2020, **11**(7), 764.
29 J. Wen, X. Tan, Y. Hu, Q. Guo and X. Hong, *Environ. Sci. Technol.*, 2017, **51**(11), 6395–6403.
30 R. Zhang, Q. Xu, S. Bai, J. Hai, L. Cheng, G. Xu and Y. Qin, *Nano Energy*, 2021, **79**, 105434.
31 D. Wang, B. Zhu, X. He, Z. Zhu, G. Hutchins, P. Xu and W. N. Wang, *Environ. Sci. Nano*, 2018, **5**, 1096–1106.
32 E. Tian, F. Xia, J. Wu, Y. Zhang, J. Li, H. Wang and J. Mo, *ACS Appl. Mater. Inter.*, 2020, **12**(26), 29383–29392.
33 C. X. Li, S. Y. Kuang, Y. H. Chen, Z. L. Wang, C. Li and G. Zhu, *ACS Appl. Mater. Inter.*, 2018, **10**(29), 24332–24338.
34 Z. Y. Huo, Y. J. Kim, I. Y. Suh, D. M. Lee, J. H. Lee, Y. Du, S. Wang, H. J. Yoon and S. W. Kim, *Nat. Commun.*, 2021, **12**(1), 3693.
35 X. Yang, H. Sun, G. Li, T. An and W. Choi, *Appl. Catal., B*, 2021, **294**, 120252.

36 H. C. Huang, H. L. Huang, Y. F. Hsu and S. Yang, *IOP Conference Series: Earth and Environmental Science*, 2019, **310**(5), 052027.
37 N. Turgeon, J. M. Vyskocil, J.-G. Turgeon and C. Duchaine, *Aerosol Sci. Tech.*, 2020, **12**, 1471–1478.
38 L. Liu, A. A. laghari, G. Meng, H. Chen, C. Wang and Y. Xue, *J. Environ. Chem. Eng.*, 2022, **10**(3), 107641.
39 G. Li, X. Nie, J. Chen, Q. Jiang, T. An, P. K. Wong, H. Zhang, H. Zhao and H. Yamashita, *Water Res.*, 2015, **86**, 17–24.
40 H. Takahashi, M. Nakazawa, C. Ohshima, M. Sato, T. Tsuchiya, A. Takeuchi, M. Kunou, T. Kuda and B. Kimura, *Sci. Rep.*, 2015, **5**, 11819.
41 A. Poormohammadi, S. Bashirian, A. R. Rahmani, G. Azarian and F. Mehri, *Environ. Sci. Pollut. Res. Int.*, 2021, **28**(32), 43007–43020.
42 S. Wu, X. Li, Y. Tian, Y. Lin and Y. H. Hu, *Chem. Eng. J.*, 2021, **406**, 126747.
43 R. T. Tadashi Matsunaga, T. Nakajima and H. Wake, *FEMS Microbiol. Lett.*, 1985, **29**, 211–214.
44 Y. Cai, T. Sun, G. Li and T. An, *ACS ES&T Eng.*, 2021, **1**(7), 1046–1064.
45 W. Wang, T. An, G. Li, D. Xia, H. Zhao, J. C. Yu and P. K. Wong, *Appl. Catal., B*, 2017, **217**, 570–580.
46 D. Xia, W. Wang, R. Yin, Z. Jiang, T. An, G. Li, H. Zhao and P. K. Wong, *Appl. Catal., B*, 2017, **214**, 23–33.
47 A. Priyadharsan, G. Palanisamy, L. Arul Pragasan, M. F. Albeshr, A. Fahad Alrefaei, J. Lee and X. Liu, *Chemosphere*, 2023, **335**, 139102.
48 A. Vohra, D. Y. Goswami, D. A. Deshpande and S. S. Block, *J. Ind. Microbiol. Biotechnol.*, 2005, **32**(8), 364–370.
49 S. M. Zacarías, M. L. Satuf, M. C. Vaccari and O. M. Alfano, *Ind. Eng. Chem. Res.*, 2012, **51**(42), 13599–13608.
50 A. Vohra, D. Y. Goswami, D. A. Deshpande and S. S. Block, *Appl. Catal., B*, 2006, **64**(1–2), 57–65.
51 S. Josset, S. Hajiesmaili, D. Begin, D. Edouard, C. Pham-Huu, M. C. Lett, N. Keller and V. Keller, *J. Hazard. Mater.*, 2010, **175**(1–3), 372–381.
52 J. Kim and J. Jang, *Aerosol Sci. Tech.*, 2018, **52**(5), 557–566.
53 E. Mirskaya and I. E. Agranovski, *Crit. Rev. Microbiol.*, 2018, **44**(6), 739–758.
54 C. Humbal, S. Gautam and U. Trivedi, *Environ. Int.*, 2018, **118**, 189–193.
55 M. Valdez Castillo and S. Arriaga, *Front. Environ. Sci. Eng.*, 2021, **15**(3), 43.
56 M. Valdez-Castillo, J. O. Saucedo-Lucero and S. Arriaga, *Chem. Eng. J.*, 2019, **374**, 914–923.
57 Q. Li, Y. Yin, D. Cao, Y. Wang, P. Luan, X. Sun, W. Liang and H. Zhu, *ACS Nano*, 2021, **15**(7), 11992–12005.
58 Y. Liu, Z. Ning, Y. Chen, M. Guo, Y. Liu, N. K. Gali, L. Sun, Y. Duan, J. Cai, D. Westerdahl, X. Liu, K. Xu, K. F. Ho, H. Kan, Q. Fu and K. Lan, *Nature*, 2020, **582**(7813), 557–560.
59 S. V. Mohan, M. Hemalatha, H. Kopperi, I. Ranjith and A. K. Kumar, *Chem. Eng. J.*, 2021, **405**, 126893.
60 L. Zhang, J. Zhang, H. Yu and J. Yu, *Adv. Mater.*, 2022, **34**(11), e2107668.
61 Y. Ma, X. Yi, S. Wang, T. Li, B. Tan, C. Chen, T. Majima, E. R. Waclawik, H. Zhu and J. Wang, *Nat. Commun.*, 2022, **13**(1), 1400.
62 S. Ali, S. Ali, P. M. Ismail, H. Shen, A. Zada, A. Ali, I. Ahmad, R. Shah, I. Khan, J. Chen, C. Cui, X. Wu, Q. Kong, J. Yi, X. Zu, H. Xiao, F. Raziq and L. Qiao, *Appl. Catal., B*, 2022, **307**, 121149.
63 S. Lu, G. Meng, C. Wang and H. Chen, *Chem. Eng. J.*, 2021, **404**, 126526.
64 P. Li, J. Li, X. Feng, J. Li, Y. Hao, J. Zhang, H. Wang, A. Yin, J. Zhou, X. Ma and B. Wang, *Nat. Commun.*, 2019, **10**(1), 2177.
65 P. Tang, Z. Zhang, A. Y. El-Moghazy, N. Wisuthiphaet, N. Nitin and G. Sun, *ACS Appl. Mater. Inter.*, 2020, **12**(44), 49442–49451.
66 A. Hernandez-Gordillo and S. Arriaga, *Catal. Lett.*, 2021, 1–12.
67 M. A. Jahne, S. W. Rogers, T. M. Holsen, S. J. Grimberg and I. P. Ramler, *Environ. Sci. Technol.*, 2015, **49**(16), 9842–9849.
68 J. Li, L. Zhou, X. Zhang, C. Xu, L. Dong and M. Yao, *Atmos. Environ.*, 2016, **124**, 404–412.
69 N. Yamamoto, D. Hospodsky, K. C. Dannemiller, W. W. Nazaroff and J. Peccia, *Environ. Sci. Technol.*, 2015, **49**(8), 5098–5106.
70 W. Wang, G. Li, D. Xia, T. An, H. Zhao and P. K. Wong, *Environ. Sci.: Nano*, 2017, **4**(4), 782–799.
71 W. Wang, L. Zhang, T. An, G. Li, H.-Y. Yip and P.-K. Wong, *Appl. Catal., B*, 2011, **108–109**, 108–116.
72 W. Wang, Y. Liu, G. Li, Z. Liu, P. K. Wong and T. An, *Environ. Int.*, 2022, **168**, 107460.
73 M. R. Hamblin, *Curr. Opin. Microbiol.*, 2016, **33**, 67–73.
74 S. M. Zacarias, S. Pirola, A. Manassero, M. E. Visuara, O. M. Alfano and M. L. Satuf, *Photochem. Photobiol. Sci.*, 2019, **18**(4), 884–890.
75 H. Wang, L. Peng, G. Li, W. Zhang, Z. Liang, H. Zhao and T. An, *Appl. Catal., B*, 2023, **324**, 122273.
76 M. Naguib, M. Kurtoglu, V. Presser, J. Lu, J. Niu, M. Heon, L. Hultman, Y. Gogotsi and M. W. Barsoum, *Adv. Mater.*, 2011, **23**(37), 4248–4253.
77 Q. Yang, Y. Wang, X. Li, H. Li, Z. Wang, Z. Tang, L. Ma, F. Mo and C. Zhi, *Energy Environ. Mater.*, 2018, **1**(4), 183–195.
78 X. Xie, M. Q. Zhao, B. Anasori, K. Maleski, C. E. Ren, J. Li, B. W. Byles, E. Pomerantseva, G. Wang and Y. Gogotsi, *Nano Energy*, 2016, **26**, 513–523.
79 M. Wen, G. Li, H. Liu, J. Chen, T. An and H. Yamashita, *Environ. Sci.: Nano*, 2019, **6**(4), 1006–1025.
80 Y. Zhang, S. Yuan, X. Feng, H. Li, J. Zhou and B. Wang, *J. Am. Chem. Soc.*, 2016, **138**(18), 5785–5788.
81 D. K. Yoo and S. H. Jhung, *ACS Appl. Mater. Inter.*, 2019, **11**(50), 47649–47657.
82 X. Ding, H. Liu, J. Chen, M. Wen, G. Li, T. An and H. Zhao, *Nanoscale*, 2020, **12**(17), 9462–9470.
83 J. Zhang, P. Li, X. Zhang, X. Ma and B. Wang, *ACS Appl. Mater. Inter.*, 2020, **12**(41), 46057–46064.
84 G. Fan, J. Zhou, X. Zheng, J. Luo, L. Hong and F. Qu, *Chemosphere*, 2020, **239**, 124721.

85 R. Ni, H. Xu, J. Ma, Q. Lu, Y. Hu, C. Huang, Q. Ke and Y. Zhao, *Mater. Today Chem.*, 2022, **23**, 100689.
86 Z. Zhu, Y. Zhang, L. Bao, J. Chen, S. Duan, S. C. Chen, P. Xu and W. N. Wang, *Environ. Sci.: Nano*, 2021, **8**(4), 1081–1095.
87 S. Yuan, L. Feng, K. Wang, J. Pang, M. Bosch, C. Lollar, Y. Sun, J. Qin, X. Yang, P. Zhang, Q. Wang, L. Zou, Y. Zhang, L. Zhang, Y. Fang, J. Li and H. C. Zhou, *Adv. Mater.*, 2018, **30**(37), e1704303.
88 V. N. Nguyen, Z. Zhao, B. Z. Tang and J. Yoon, *Chem. Soc. Rev.*, 2022, **51**(9), 3324–3340.
89 M. Tavakkoli Yaraki, B. Liu and Y. N. Tan, *Nanomicro. Lett.*, 2022, **14**(1), 123.
90 Y. B. Ji, W. J. Chen, T. Z. Shan, B. Y. Sun, P. C. Yan and W. Jiang, *Chem. Biodivers.*, 2020, **17**(2), e1900640.
91 K. J. Heo, S. B. Jeong, J. Shin, G. B. Hwang, H. S. Ko, Y. Kim, D. Y. Choi and J. H. Jung, *Nano Lett.*, 2021, **21**(4), 1576–1583.
92 H. A. Foster, I. B. Ditta, S. Varghese and A. Steele, *Appl. Microbiol. Biotechnol.*, 2011, **90**(6), 1847–1868.
93 N. A. Daub, F. Aziz, M. Aziz, J. Jaafar, W. N. W. Salleh, N. Yusof and A. F. Ismail, *Water Air Soil Poll.*, 2020, **231**(9), 461.
94 J. W. Liou and H. H. Chang, *Arch. Immunol. Ther. Exp. (Warsz)*, 2012, **60**(4), 267–275.
95 T. Tatsuma, S.-i Tachibana and A. Fujishima, *J. Phys. Chem. B*, 2001, **105**, 6987–6992.
96 Y. Yang, X. Wu, L. Ma, C. He, S. Cao, Y. Long, J. Huang, R. D. Rodriguez, C. Cheng, C. Zhao and L. Qiu, *Adv. Mater.*, 2021, **33**(8), e2005477.
97 Y. Yu, Y. He, Z. Mu, Y. Zhao, K. Kong, Z. Liu and R. Tang, *Adv. Funct. Mater.*, 2019, **30**(6), 19085.
98 Q. Wang, P. Xiao, W. Zhou, Y. Liang, G. Yin, Q. Yang, S. W. Kuo and T. Chen, *Nanomicro. Lett.*, 2022, **14**(1), 62.
99 F. Pan, Z. Liu, B. Deng, Y. Dong, X. Zhu, C. Huang and W. Lu, *Nanomicro. Lett.*, 2021, **13**(1), 43.
100 Y. Tang, H. Sun, Z. Qin, S. Yin, L. Tian and Z. Liu, *Chem. Eng. J.*, 2020, **398**, 125575.
101 B. K. Ahn, *J. Am. Chem. Soc.*, 2017, **139**(30), 10166–10171.
102 H. Lee, S. M. Dellatore, W. M. Miller and P. B. Messersmith, *Science*, 2007, **318**, 426–430.
103 C. Hu, L. Long, J. Cao, S. Zhang and Y. Wang, *Chem. Eng. J.*, 2021, **411**, 128564.
104 Y. Zheng, H. Bai, Z. Huang, X. Tian, F. Q. Nie, Y. Zhao, J. Zhai and L. Jiang, *Nature*, 2010, **463**(7281), 640–643.
105 L. Peng, H. Wang, G. Li, W. Zhang, Z. Liang and T. An, *Appl. Catal., B*, 2023, **329**, 122580.
106 H. Venkatesan, J. Chen, H. Liu, W. Liu and J. Hu, *Adv. Funct. Mater.*, 2020, **30**(30), 2002437.
107 X. Tian, H. Bai, Y. Zheng and L. Jiang, *Adv. Funct. Mater.*, 2011, **21**(8), 1398–1402.
108 Y. Liu, N. Yang, X. Li, J. Li, W. Pei, Y. Xu, Y. Hou and Y. Zheng, *Small*, 2020, **16**(9), e1901819.
109 H. Liu, Y. Wang, W. Yin, H. Yuan, T. Guo and T. Meng, *J. Mater. Chem. A*, 2022, **10**(13), 7130–7137.
110 H. Shen, M. Han, Y. Shen and D. Shuai, *ACS Environ. Au*, 2022, **2**(4), 290–309.
111 L. Peng, H. Wang, G. Li, Z. Liang, W. Zhang, W. Zhao and T. An, *Nat. Commun.*, 2023, **14**(1), 2412.
112 J. Xiao, J. Rabeah, J. Yang, Y. Xie, H. Cao and A. Brückner, *ACS Catal.*, 2017, **7**(9), 6198–6206.
113 J. Xiao, Q. Han, Y. Xie, J. Yang, Q. Su, Y. Chen and H. Cao, *Environ. Sci. Technol.*, 2017, **51**(22), 13380–13387.
114 Y. Sun, S. Qiu, Z. Fang, J. Yang, X. Song and S. Xiao, *ACS Sustainable. Chem. Eng.*, 2023, **11**(8), 3359–3369.
115 N. Liu, J. Ming, A. Sharma, X. Sun, N. Kawazoe, G. Chen and Y. Yang, *Chem. Eng, J.*, 2021, **426**, 131217.
116 A. A. Laghari, G. Jiang, D. H. Kalhoro, C. Hong and C. Wang, *Aerosol Sci. Tech.*, 2022, **57**(1), 12–23.
117 C. Wang, Z. W. Zhang and H. Liu, *J. Hazard. Mater.*, 2019, **366**, 27–33.
118 Q. Zhang, B. Damit, J. Welch, H. Park, C. Y. Wu and W. Sigmund, *J. Aerosol Sci.*, 2010, **41**(9), 880–888.
119 Y. Wu and M. Yao, *J. Aerosol Sci.*, 2010, **41**(7), 682–693.
120 S. O. P. Amrita Pal, L. E. Yu and M. B. Ray, *Ind. Eng. Chem. Res.*, 2008, **47**, 7580–7585.
121 J. Cao, Z. Cheng, L. Kang, M. Lin and L. Han, *RSC Adv.*, 2020, **10**(34), 20155–20161.
122 L. Liu, G. Meng, A. A. Laghari, H. Chen, C. Wang and Y. Xue, *J. Hazard. Mater.*, 2022, **429**, 128311.
123 Y. Ahmadi, N. Bhardwaj, K. H. Kim and S. Kumar, *Sci. Total Environ*, 2021, **794**, 148477.
124 Y. Gao, E. Tian and J. Mo, *ACS ES&T Engg*, 2021, **1**(10), 1449–1459.
125 I. Danilenko, O. Gorban, P. M. da Costa Zaragoza de Oliveira Pedro, J. Viegas, O. Shapovalova, L. Akhkozov, T. Konstantinova and S. Lyubchyk, *Top. Catal.*, 2020, **64**(13–16), 772–779.
126 G. Q. Gu, C. B. Han, C. X. Lu, C. He, T. Jiang, Z. L. Gao, C. J. Li and Z. L. Wang, *ACS Nano*, 2017, **11**(6), 6211–6217.
127 Y. C. Chen, C. H. Liao, W. T. Shen, C. Su, Y. C. Wu, M. H. Tsai, S. S. Hsiao, K. P. Yu and C. H. Tseng, *Indoor Air*, 2019, **29**(3), 439–449.
128 A. Dutheil de la Rochere, A. Evstratov, S. Bayle, L. Sabourin, A. Frering and J. M. Lopez-Cuesta, *PLoS One*, 2019, **14**(10), e0224114.
129 Y. Lu, S. Guan, L. Hao, H. Yoshida, S. Nakada, T. Takizawa and T. Itoi, *Sci. Rep.*, 2022, **12**(1), 16038.
130 R. M. Moattari, T. Mohammadi, S. Rajabzadeh, H. Dabiryan and H. Matsuyama, *J. Taiwan Inst. Chem. E*, 2021, **122**, 284–310.
131 M. Naeimirad, A. Zadhoush, R. Kotek, R. Esmaeely Neisiany, S. Nouri Khorasani and S. Ramakrishna, *J. Appl. Polym. Sci.*, 2018, **135**(21), 46265.
132 S. Li, R. Zhang, J. Xie, D. E. Sameen, S. Ahmed, J. Dai, W. Qin, S. Li and Y. Liu, *Appl. Surf. Sci.*, 2020, **533**, 147516.
133 Y. Bian, S. Wang, L. Zhang and C. Chen, *Build. Environ.*, 2020, **170**, 106628.
134 S. J. Baldwin, P. D. Slaine, E. Keltie, S. Palit, S. L. McKinnell, B. E. Longpré, K. R. Ko, J. Green, G. Markle, J. S. Kim, C. McCormick and J. P. Frampton, *ACS Appl. Polym. Mater.*, 2021, **3**(8), 4245–4255.
135 S. M. Zacarías, A. Manassero, S. Pirola, O. M. Alfano and M. L. Satuf, *Environ. Sci. Pollut. Res.*, 2021, **28**(19), 23859–23867.
136 S. Josset, J. Taranto, N. Keller, V. Keller and M. C. Lett, *Environ. Sci. Technol.*, 2010, **44**(7), 2605–2611.

137 S. Pigeot-Remy, J. C. Lazzaroni, F. Simonet, P. Petinga, C. Vallet, P. Petit, P. J. Vialle and C. Guillard, *Appl. Catal., B*, 2014, **144**, 654–664.
138 P. Chuaybamroong, R. Chotigawin, S. Supothina, P. Sribenjalux, S. Larpkiattaworn and C.-Y. Wu, *Indoor Air*, 2010, **20**(3), 246–254.
139 T. Mousavi, F. Golbabaei, M. H. Kohneshahri, M. R. Pourmand, S. Rezaie, M. Hosseini and A. Karimi, *Pollution*, 2021, **7**(2), 309–319.
140 A. Pal, X. Min, L. E. Yu, S. O. Pehkonen and M. B. Ray, *Int. J. Chem. React. Eng.*, 2005, **3**(1), A45.
141 M. B. Marcó, A. C. Negro, O. M. Alfano and A. D. Quiberoni, *Environ. Sci. Pollut. Res.*, 2018, **25**(22), 21385–21392.
142 A. Pal, S. O. Pehkonen, L. E. Yu and M. B. Ray, *Ind. Eng. Chem. R*, 2008, **47**(20), 7580–7585.
143 N. Doss, G. Carré, V. Keller, P. André and N. Keller, *Water Air Soil Poll.*, 2018, **229**(2), 29.
144 T. Daikoku, M. Takemoto, Y. Yoshida, T. Okuda, Y. Takahashi, K. Ota, F. Tokuoka, A. T. Kawaguchi and K. Shiraki, *Aerosol Air Qual. Res.*, 2015, **15**(4), 1469–1484.
145 K. Shiraki, H. Yamada, Y. Yoshida, A. Ohno, T. Watanabe, T. Watanabe, H. Watanabe, H. Watanabe, M. Yamaguchi, F. Tokuoka, S. Hashimoto, M. Kawamura and N. Adachi, *Aerosol Air Qual. Res.*, 2017, **17**(11), 2901–2912.
146 Y. Yao, T. Ochiai, H. Ishiguro, R. Nakano and Y. Kubota, *Appl. Catal., B*, 2011, **106**(3), 592–599.
147 C. H. Lin, J. W. Lee, C. Y. Chang, Y. J. Chang, Y. C. Lee and M. Y. Hwa, *Surf. Coat. Tech.*, 2010, **205**, S341–S344.
148 S. Josset, S. Hajiesmaili, D. Begin, D. Edouard, C. Pham-Huu, M.-C. Lett, N. Keller and V. Keller, *J. Hazard. Mater.*, 2010, **175**(1), 372–381.
149 C. Rodrigues-Silva, S. M. Miranda, F. V. S. Lopes, M. Silva, M. Dezotti, A. M. T. Silva, J. L. Faria, R. A. R. Boaventura, V. J. P. Vilar and E. Pinto, *Environ. Sci. Pollut. R*, 2017, **24**(7), 6372–6381.
150 M. Valdez-Castillo, J. O. Saucedo-Lucero, K. L. Villalobos-Romero, F. Pérez-Rodriguez and S. Arriaga, *Environ. Sci. Pollut. Res.*, 2021, **28**(11), 13970–13980.
151 M. Valdez-Castillo and S. Arriaga, *Front. Environ. Sci. Eng.*, 2021, **15**(3), 1–13.
152 T. D. Pham and B. K. Lee, *Appl. Surf. Sci.*, 2014, **296**, 15–23.
153 E. W. Moon, H. W. Lee, J. H. Rok and J. H. Ha, *Sci. Total Environ*, 2020, **749**, 141574.
154 T. D. Pham and B. K. Lee, *Chem. Eng. J.*, 2016, **286**, 377–386.
155 A. Vohra, D. Y. Goswami, D. A. Deshpande and S. S. Block, *J. Ind. Microbiol. Biotech.*, 2005, **32**(8), 364.
156 T. D. Pham and B. K. Lee, *J. Solid State Chem.*, 2015, **232**, 256–263.
157 J. H. Martínez-Montelongo, I. E. Medina-Ramírez, Y. Romo-Lozano and J. A. Zapien, *Chemosphere*, 2020, **257**, 127236.
158 E. A. Kozlova, A. S. Safatov, S. A. Kiselev, V. Y. Marchenko, A. A. Sergeev, M. O. Skarnovich, E. K. Emelyanova, M. A. Smetannikova, G. A. Buryak and A. V. Vorontsov, *Environ. Sci. Technol.*, 2010, **44**(13), 5121–5126.
159 S. P. Tallósy, L. Janovák, J. Ménesi, E. Nagy, Á. Juhász, L. Balázs, I. Deme, N. Buzás and I. Dékány, *Environ. Sci. Pollut. Res.*, 2014, **21**(19), 11155–11167.
160 S. Lu, G. Meng, C. Wang and H. Chen, *Chem. Eng. J.*, 2021, **404**, 126526.
161 L. Liu, G. Meng, A. A. Laghari, H. Chen, C. Wang and Y. Xue, *J. Hazard. Mater.*, 2022, **429**, 128311.
162 L. Liu, A. A. laghari, G. Meng, H. Chen, C. Wang and Y. Xue, *J. Environ. Chem. Eng.*, 2022, **10**(3), 107641.
163 E. F. Mohamed and G. Awad, *Environ. Sci. Pollut. Res.*, 2020, **27**(19), 24507–24517.
164 T. Cao, Y. Zheng, H. Dong, S. Wang, Y. Zhang and Q. Cong, *Agr., Ecosyst. Environ.*, 2023, **342**, 108221.
165 A. Hernandez-Gordillo and S. Arriaga, *Catal. Lett.*, 2022, **152**(3), 629–640.
166 Y. Xie, X. Zhu, P. Zhang, S. Wang, J. Yang and J. Li, *Chem. Eng. J.*, 2023, **454**, 140231.
167 Y. Zhao, A. J. Aarnink and H. Xin, *J. Air. Waste Manag. Assoc.*, 2014, **64**(1), 38–46.
168 M. Valdez-Castillo, J. O. Saucedo-Lucero, K. L. Villalobos-Romero, F. Perez-Rodriguez and S. Arriaga, *Environ. Sci. Pollut. Res.*, 2021, **28**(11), 13970–13980.
169 D. M. Schultz and T. P. Yoon, *Science*, 2014, **343**(6174), 1239176.
170 H. Sun, Z. Jiang, D. Wu, L. Ye, T. Wang, B. Wang, T. An and P. K. Wong, *ChemSusChem*, 2019, **12**(4), 890–897.
171 R. Zhang, C. Song, M. Kou, P. Yin, X. Jin, L. Wang, Y. Deng, B. Wang, D. Xia, P. K. Wong and L. Ye, *Environ. Sci. Technol.*, 2020, **54**(6), 3691–3701.
172 S. F. Dehghan, F. Golbabaei, T. Mousavi, H. Mohammadi, M. H. Kohneshahri and R. Bakhtiari, *Pollution*, 2020, **6**(1), 185–196.
173 L. Gorvel, M. Yver, E. Robert, M. Harmant, M. Rosa-Calatrava, B. Lina, J. P. Gorvel, V. Moulès, R. Albalate and C. Gaüzère, *Clean – Soil Air Water*, 2014, **42**(6), 703–712.
174 G. Z. Ramon and E. M. V. Hoek, *J. Membr. Sci.*, 2012, **392–393**, 1–8.
175 Z. Zhang, A. Y. El-Moghazy, N. Wisuthiphaet, N. Nitin, D. Castillo, B. G. Murphy and G. Sun, *ACS Appl. Mater. Inter.*, 2020, **12**(44), 49416–49430.
176 H. He, X. Dong, M. Yang, Q. Yang, S. Duan, Y. Yu, J. Han, C. Zhang, L. Chen and X. Yang, *Catal. Commun.*, 2004, **5**(3), 170–172.
177 F. Wang, T. Hou, X. Zhao, W. Yao, R. Fang, K. Shen and Y. Li, *Adv. Mater.*, 2021, **33**(35), e2102690.
178 L. Jiang, X. Yuan, G. Zeng, J. Liang, Z. Wu and H. Wang, *Environ. Sci.: Nano*, 2018, **5**(3), 599–615.
179 Z. Zhao, Y. Zheng, C. Wang, S. Zhang, J. Song, Y. Li, S. Ma, P. Cheng, Z. Zhang and Y. Chen, *ACS Catal.*, 2021, **11**(4), 2098–2107.
180 Y. Guo, Q. Zhou, B. Zhu, C. Y. Tang and Y. Zhu, *EES Cataly.*, 2023, **1**, 333.
181 Q. Zhong, Y. Li and G. Zhang, *Chem. Eng. J.*, 2021, **409**, 128099.
182 L. Lyu, S. Cho and Y. M. Kang, *EES Catal.*, 2023, **1**, 230.
183 C. Liu, Q. Zhang and Z. Zou, *J. Mater. Sci. Tech.*, 2023, **139**, 167–188.